Journal Pre-proof

Two-process constitutive model for semicrystalline polymers across a wide range of strain rates

Michael I. Okereke, Ambrose I. Akpoyomare
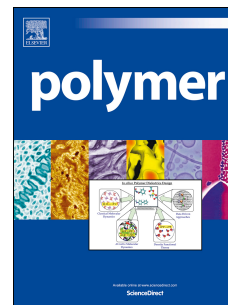
Please cite this article as: Okereke MI, Akpoyomare AI, Two-process constitutive model for semicrystalline polymers across a wide range of strain rates, *Polymer* (2019), doi: https://doi.org/10.1016/j.polymer.2019.121818.

This is a PDF file of an article that has undergone enhancements after acceptance, such as the addition of a cover page and metadata, and formatting for readability, but it is not yet the definitive version of record. This version will undergo additional copyediting, typesetting and review before it is published in its final form, but we are providing this version to give early visibility of the article. Please note that, during the production process, errors may be discovered which could affect the content, and all legal disclaimers that apply to the journal pertain.

Two-process constitutive model for semicrystalline polymers across a wide range of strain rates.

Michael I. Okereke[a,*], Ambrose I. Akpoyomare[a]

[a]*Department of Engineering Science, University of Greenwich, Kent, United Kingdom*

Abstract

The presence of crystalline and amorphous phases in semicrystalline polymers presents interesting constitutive modelling challenges. In this study, a physically based, three-dimensional constitutive model has been developed for simulating a wide range of features observed in deformation and processing of semicrystalline polymers. The proposed model combines into one constitutive model such features as: multiple viscoelastic relaxation processes, very wide strain-rate range, temperature-dependence, adiabatic heating, structural rejuvenation; in addition to it being applied to a semicrystalline polymer. The constitutive mathematics is based on a one-process *glass-rubber* model for amorphous polymers. It adapts that model to semicrystalline polymers by extending it to two relaxation processes: one associated with the glass transition of the mobile amorphous phase; the other associated with relaxation of the crystalline fraction and its associated rigid amorphous phase. In particular, two dominant processes were identified: the α-process and the β-process. The model has been implemented numerically into a commercial finite element code through a user-defined material subroutine (UMAT). The model has been validated against compression test results carried out on polypropylene. Also, the model predicts very well the experimentally observed nonlinear rate-dependent response and post-yield de-ageing of polypropylene.

Keywords: semicrystalline polymers, polypropylene, constitutive modeling, nonlinear rate-dependent response

1. Introduction

The varied uses of polymers and polymer-based materials in structural designs have become commonplace. This is helped by advances in material science, processing techniques and the development of predictive models to predict, reliably, the constitutive responses of the polymeric constituents. The modelling of polymers is complicated by their diverse nonlinear phenomena which have been widely reported in literature[1, 2, 3].

Corresponding Address: Department of Engineering Science, University of Greenwich, Medway Campus, Kent, ME4 4TB, United Kingdom Phone: +44 (0) 1634 88 3580 Fax: +44 (0) 1634 88 3153.

Email address: `m.i.okereke@gre.ac.uk` (Michael I. Okereke)

The abundance of research into the physics of polymer deformation has increased the understanding of the origin of the many nonlinear phenomena of polymers. Several simple models have been developed to model different features of the polymer behaviour. It remains a key objective to develop a robust predictive tool that captures the whole range of mechanical responses of solid polymers ranging from linear elastic, viscoelastic, viscoplastic to several nonlinear viscoelastic and post-yield phenomena.

A lot has been published on the constitutive modelling of amorphous polymers. Some of the widely cited authors are Haward[4, 5], Boyce and co-workers[6, 7, 8], Meijer and co-workers[9] as well as the so-called *glass-rubber model* [10, 11, 12]. The amorphous polymers are monophasic while semicrystalline polymers (SCPs) are multiphasic consisting of *mobile amorphous, crystalline* and *rigid amorphous fractions/phases*. Unlike the amorphous polymers, the multi-phase structures of semicrystalline polymers present a significant complication in understanding and quantitatively describing their plastic deformation.

The microstructure of a semicrystalline polymers is composed mainly of lamellar crystallites (typically 20% to 80% by volume) embedded within a matrix of amorphous macromolecular system. The crystalline system act as tie molecules and bind the amorphous phase together. Also, there exists a third phase called the rigid amorphous fraction, which shows kinetics distinct from the crystalline or amorphous phases [13]. Stacks of layered lamellae are typically the basic building blocks of spherulites. These units link with one another to form a hierarchical superstructure of the semicrystalline polymer [14]. Therefore, the constitutive behaviour of semicrystalline polymers is intrinsically linked to the viscoelastic behaviour of the underlying microstructure. Understanding the deformation mechanisms of these in relation to their observed macroscale deformation kinetics is central to reliable prediction of the constitutive behaviour of semicrystalline polymers.

The earliest models to exploit the principle described above were pioneered by works of such authors as Hay and Keller[15], Peterlin[16, 17], Schultz [18], and Galeski *et al.* [19], amongst others. These pioneers opined that the plastic deformation of semicrystalline polymers involves several mechanics of deformation of the crystalline and amorphous phases for example: slip along certain crystallographic planes, twinning, martensite transformations, interlamellar sliding and even lamellar separation [20]. The limitations from these microstructure-based models lie in the fact that they tend to only predict deformations along simple loading paths, and cannot quantitatively describe stress-strain curves arising from complex loading conditions (e.g. load-unload) as well as the microstructural transformations induced by the deformations of the different phases [21]. To date, there remains the research gap of developing a holistic constitutive model for SCPs capable of capturing complex loading history and microstructural transformations arising from the distinct mechanisms of the individual phases of SCPs across a wide range of strain rates, temperature regimes and post-yield mechanics.

In the last two decades, several research efforts have been directed towards constitutive modelling of semicrystalline polymers. The existing constitutive models can be classed in three dominant categories: the composite-mechanics models [22]; the lamella-[23, 24, 25] and

2

crystal-plasticity models [26]; and finally, the polymer macromolecular deformation models [27, 28, 29, 30, 31, 32]. The composite-mechanics models apply the modelling principles of composite materials to describe constitutive models for SCPs. The amorphous polymer is described as the matrix system while the crystalline phases are considered as reinforcing inclusions. Such models are known to predict reliably linear viscoelastic behaviour of SCPs, but at finite strains and post-yield deformation, the models fail to capture the complex nonlinear responses of semicrystalline polymers.

Also, the lamella- and crystal-plasticity models focus on describing deformation of the complex microstructure of semicrystalline polymers, using metal plasticity arguments. They also are quite good at predicting small-strain, quasi-static responses of these polymers how-ever, as the microstructure evolves under load following breakup of the spherulitic structure of the SCPs, these models fail to capture the observed mechanical response.

The third modelling category is the most promising and exploits the polymer macro-molecular deformation kinetics. Quite a lot of publications already exist for monophasic (amorphous) systems and such models can be adapted to capture the unique features of SCPs. Here, we consider a few of these models. Bardenhagen and co-workers [33] proposed a 3D finite deformation viscoplastic model by the addition of stresses which relates to vis-coelastic and elastic-plastic constitutive model components. The model has been used by Hasanpour and Ziaei-Rad [34] to describe the nonlinear material behaviour of polytetraflu-oroethylene (PTFE).

Hong and co-workers [35, 36] also proposed a tensile-deformation-only *three-component model* of SCPs. The authors postulated that the cumulative tensile deformation response of SCPs can be divided into three constituent quasi-static stresses arising from: a relax-ing stress, σ_r; a crystal block stress, σ_c; and a network stress, σ_n. The model was vali-dated reliably using experiments carried out on ultra-high molecular weight polyethylene (UHMWPE). This modelling approach is motivated by the need to address the structural complexity of SCPs.

Also, another model that has found wide application in describing the plastic deforma-tion of semicrystalline polymers is the so-called *interpenetration network model* [37, 38, 14]. The model is suitable for describing the constitutive behaviour of melt-crystallized semicrys-talline polymers made by quenching, for example. According to the model, the polymer is composed of a rigid *crystal network* that penetrates a soft *crystallite of enhanced amorphous matrix network* [39, 38]. The crystal block is formed by a small portion of crystallites which adhere to one another through a network of intercrystalline links [40]. The crystal network deformation (during necking) is governed by a Takayanagi tie molecule model [41] while the deformation of the amorphous network follows an affine deformation provided the elongation temperature (T_E) is above the glass transition temperature (T_g) of the amorphous phase [38]. The interpenetrating model is essentially a network model in which the macromolecular net-work strands of the amorphous phase have their ends anchored by either entanglements or stacks of rigid crystallites. The interpenetrating network model therefore derives its name from such interpenetrated networks of crystalline and amorphous networks. Unfortunately,

this model has neglected the contributions of the *rigid amorphous fraction* to SCPs response.

A promising approach used to describe deformation of amorphous polymers over a wide range of strain-rates is based on the viscoelastic relaxations of polymers. Mulliken and Boyce [7] used this approach to model the nonlinear viscoelasticity of polycarbonate and poly(methyl methacrylate) across a wide range of strain rates. The approach uses the Ree-Eyring multi-process relaxation kinetics to model the mechanical behaviour of the polymer. Here, we posit that a similar approach can be applied to semicrystalline polymers. In fact, Jourdan *et al.* [42] showed that the $\beta-$relaxation of SCPs is related to the glass-transition of the wholly amorphous segment. The mechanical response of this segment shows high rubbery plateau in the shear modulus: an indication of a high cross-linking effect.

The $\alpha-$relaxation has been shown experimentally to originate within the crystalline phase and associated constrained amorphous layers [43, 44], with the later commonly described in literature as the *rigid amorphous fraction* [13, 45]. The strain-hardening response is dominated by the rubbery response of stretched amorphous segment and so not necessarily a function of the crystallinity of the polymer. Therefore, there exists a link between the viscoelastic relaxations and the holistic mechanical behaviour of SCPs. This observation will be exploited in development of the two-process constitutive model for SCPs.

Most of the existing constitutive models for SCPs were validated using polyethylene as test composite. Studies involving use of polypropylene as test case for the proposed predictive models are quite few. One of such is the work of Sweeney and co-workers[46] who proposed a constitutive model for prediction of large deformation of polypropylene under multiaxial loading and processing conditions. The model assumes a mechanical analogue of two parallel *arms*: the first, a single Eyring process in series with an Edwards-Vilgis network and another second arm represented by entirely an Edwards-Vilgis network. Nevertheless, there remains a need for a holistic constitutive model for SCPs, capturing the distinctive features of polypropylene across a wide range of mechanical responses (linear viscoelasticity to post-yield), temperatures, strain rates and crystallinities. The aim of this paper is to suggest such a model. In order for the model to be able to encompass the highest strain rates, it is presented here in an adiabatic form.

There are three clearly resolved viscoelastic relaxations associated with polypropylene namely: α-, β-, and γ-relaxations and a possible δ-relaxation have all been observed [47, 48]. On a plot of $\tan\delta$ versus temperature, the relaxations appear as α-, β-, and γ-loss peaks at temperatures of 50^oC, 0^oC and -70^oC respectively[49]. McCrum, *et al.* [50] observed that the dominant relaxation for PP is the β-relaxation. This β-relaxation is associated with low temperatures or high strain rates experiments while the α-relaxation dominate high temperatures or low strain rates studies. Therefore, in the temperature window for room temperature (e.g. 20^oC - 30^oC), the polymer is in this window of dominant interaction between the α- and β-relaxations. Most practical uses of polypropylene are usually within this temperature window. As a result, this study aims to develop a constitutive model that describes the constitutive response of polypropylene across these two dominant relaxations.

4

1   This paper presents a holistic model for semicrystalline polymers using polypropylene
2   as a test case. The proposed constitutive mathematics is based on the one-process *Glass-*
3   *rubber (GR) constitutive model* [10] developed previously for amorphous polymers. In this
4   communication, we propose extending the GR model into a *two-process* version capable
5   of describing the constitutive responses of SCPs. The proposed adaptation is based on
6   the well-documented evidence from Bauwens-Crowet[51] that the mechanical behaviour of
7   many polymeric systems is a consequence of multiple processes linked to the viscoelastic
8   relaxations within the material. The model has been validated against compression tests
9   results of polypropylene obtained across a wide range of strain rates.
10

2. Model formulation

2.1. The proposed mechanical analogue

13   A one-dimensional analogue of the isochoric portion of the proposed model for SCPs
14   is shown in *Figure 1*. It consists of two viscoelastic arms (spring-dashpot arrangement)
15   for the α- and β-relaxations as well as a rubbery network spring. The stress tensor, $\boldsymbol{\sigma}$
16   associated with the deformation is a parallel response of the three parts of the model.
17   The first contribution results from the amorphous phase. Such assumption agrees with
18   the conclusions of McCrum *et al.* [49], who described β-relaxation as associated with the
19   amorphous phase.
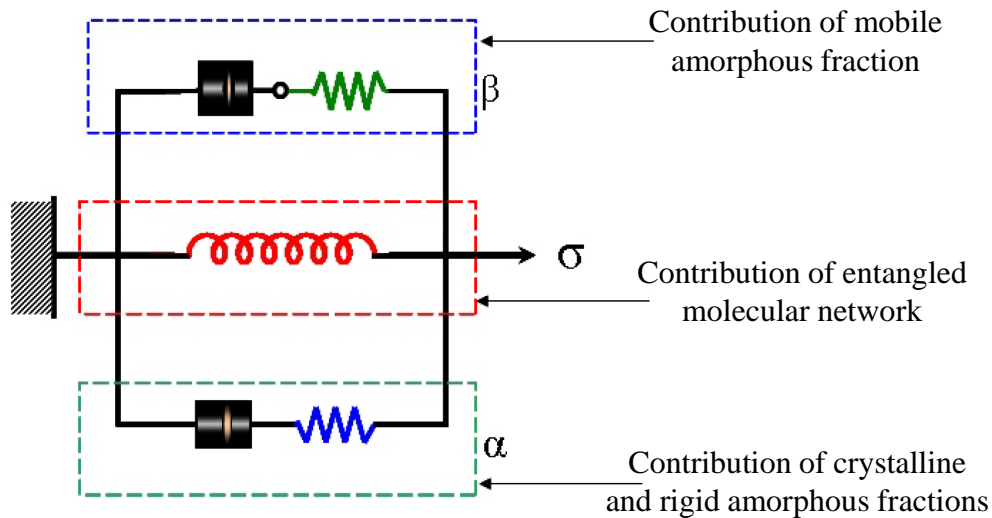
Figure 1: A three-arm one-dimensional mechanical analogue of the isochoric response of the proposed model.

20   In considering the viscoelastic relaxations of the different phases of the semicrystalline
21   polymer, it would be ideal to distinguish precisely the contributions of the purely amorphous,
22   the purely crystalline and the rigid amorphous fraction (RAF) phases. Although clear dis-
23   tinction exists between the predominantly amorphous and predominantly crystalline phases,
24   however, there is no published information, known to the authors, that clearly identifies the
25   distinction between the RAF and the other phases. Also, the microstructure of the RAF
26   is not clearly understood and it is difficult to classify it as either predominantly crystalline

5

1 or amorphous. This is because the RAF is a bridge between the amorphous and crystalline
2 phases and results in a gradation of viscoelastic relaxation effects from dominant amorphous
3 zone to a purely crystalline zone.

4

5 Therefore, for the purpose of the proposed model, the crystalline contribution has been
6 grouped together with the rigid amorphous fraction (RAF): both contributing to the $\alpha-$relaxation
7 dynamics. This is because published literature on recent fast scanning calorimetry data has
8 shown the RAF viscoelastic relaxation to be closely associated with those of the crystalline
9 fraction [45]. The approach used here has also been adopted by Brusselle-Dupend and
10 Cangemi [27, 52]. The proposed constitutive model therefore integrates the contributions of
11 these two predominant relaxations/processes and this is the basis for describing the model
12 as a *Two-process constitutive model.*

13

14 *2.2. Kinematics considerations*

15 Consider a deforming polymer continuum $\mathcal{B}$, such that $\Omega_0 \subset \mathbb{R}^3$ is defined as its natural
16 reference configuration. Let $\mathbf{x} \in \mathcal{B}$ denote the deformed position of a material particle of
17 the body given its reference/undeformed position defined by $\mathbf{X} \in \Omega_0$. At a given time, t
18 the two domains can be mapped according to $\mathbf{x} = \chi(\mathbf{X})$ [53]. The displacement field is fully
19 prescribed by a deformation gradient tensor, $\mathbf{F}(\mathbf{X})$ defined as:

$$\mathbf{F} = \nabla \mathbf{x} = \frac{\partial \mathbf{x}}{\partial \mathbf{X}}, \tag{1}$$

20 where $\boldsymbol{\nabla}$ is the vector differential operator of $\mathbf{x}$. The deformation gradient, $\mathbf{F}$ consists
21 of volumetric and isochoric parts. The former contributes to volume change while the later
22 to shape change.

23

24 Let us define respectively, the volume ratio, J, the isochoric component, $\overline{\mathbf{F}}$, and mean
25 stress, σ_m, according to *Equation 2*.

$$J = \det\mathbf{F}, \qquad \overline{\mathbf{F}} = J^{-\frac{1}{3}}\mathbf{F}, \quad \text{and} \quad \sigma_m = K \ln J \tag{2}$$

26 where $K =$ bulk modulus. The nonlinear finite deformation response of the polymer is
27 contained within the isochoric part of the deformation gradient, $\overline{\mathbf{F}}$. This isochoric defor-
28 mation gradient can be further expressed in terms of pure rotation, $\mathbf{R}$ and deviatoric left
29 stretch, $\overline{\mathbf{V}}$.

30

31 Finally, the corresponding isochoric components of deformation gradient, $\mathbf{F}$, left Cauchy-
32 Green tensor, $\overline{\mathbf{B}}$, velocity gradient, $\overline{\mathbf{L}}$ and the latter's symmetric and skew-symmetric parts
33 are given in *Equation 3*. Note that $\overline{\mathbf{D}} =$ isochoric component of the rate of deformation
34 tensor.

$$\overline{\mathbf{F}} = \overline{\mathbf{V}}\mathbf{R}, \qquad \overline{\mathbf{L}} = \dot{\overline{\mathbf{F}}}\,\overline{\mathbf{F}}^{-1}, \qquad \overline{\mathbf{B}} = \overline{\mathbf{F}}\,\overline{\mathbf{F}}^{T},$$

$$\mathbf{W} = \text{skew}\{\overline{\mathbf{L}}\} = \tfrac{1}{2}\{\overline{\mathbf{L}} - \overline{\mathbf{L}}^{T}\} \quad \text{and} \quad \overline{\mathbf{D}} = \text{sym}\{\overline{\mathbf{L}}\} = \tfrac{1}{2}\{\overline{\mathbf{L}} + \overline{\mathbf{L}}^{T}\}. \tag{3}$$

35

36

6

¹ *2.3. The constitutive mathematics*

²   The proposed constitutive model consists of a set of simultaneous equations whose solu-
³ tion gives the Cauchy stress, $\boldsymbol{\sigma}$, in terms of the deformation gradient, $\mathbf{F}$, and the isochoric
⁴ rate of deformation, $\overline{\mathbf{D}}$. The Cauchy stress, $\boldsymbol{\sigma}$, is decomposed into two components: *devia-*
⁵ *toric stress*, $\mathbf{S}$, and *mean stress*, σ_m. Therefore, the total stress acting on a polymer segment
⁶ at any given time is expressible as:

$$\boldsymbol{\sigma} = \mathbf{S} + \sigma_m \boldsymbol{I}, \qquad \text{where} \qquad \sigma_m = \tfrac{1}{3} tr(\boldsymbol{\sigma}). \tag{4}$$

⁷   To determine the expression for the deviatoric component of Cauchy stress, $\mathbf{S}$ the ar-
⁸ guments posed in the *glass-rubber* (GR) model for amorphous polymers [10, 54, 55, 11, 12]
⁹ have been adopted here. The authors postulated that the total deviatoric stress experienced
¹⁰ by a given polymer results from two key stress contributions namely:

¹¹   ○ The *bond-stretching* deviatoric stress component, $\mathbf{S}^b$, which arises from perturbation
¹²   of inter-atomic potentials. This component relaxes by thermally activated flow of
¹³   molecular segments. The flow mechanism is governed by the Eyring rate kinetics
¹⁴   through a stress-dependent viscosity.

¹⁵   ○ The *conformational* deviatoric stress component, $\mathbf{S}^c$, which arises from entropy-elastic
¹⁶   perturbation of molecular conformations. This component is defined in terms of iso-
¹⁷   tropic hyperelasticity.

¹⁸   The total stress experienced by the specimen, $\boldsymbol{\sigma}$, according to the proposed model
¹⁹ will comprise of an additive combination of the $\alpha-$process, $\boldsymbol{S}^b_\alpha$ and $\beta-$process, $\boldsymbol{S}^b_\beta$ bond-
²⁰ stretching deviatoric stress tensors; the conformational deviatoric stress tensor, $\boldsymbol{S}^c$, (*Equa-*
²¹ *tions 19* and *20*), as well as the mean stress term, σ_m (see *Equation 29*). The total stress
²² tensor is given in *Equation 5*,

$$\boldsymbol{\sigma} = \boldsymbol{S}^b_\alpha + \boldsymbol{S}^b_\beta + \boldsymbol{S}^c + \sigma_m \boldsymbol{I} \tag{5}$$

²³ where $\boldsymbol{I}$ = an identity matrix. For SCPs like polyethylene (PE), polypropylene (PP) and
²⁴ polyoxymethylene (POM), which show two relaxation processes, α and β, in the temper-
²⁵ ature/strain rate range of interest, we hereby propose a modification of the underlying
²⁶ constitutive mathematics of the *glass-rubber model* [10], for such biphasic multi-relaxation
²⁷ semicrystalline polymers. In the following sections, the model formulations for $\mathbf{S}^b$ and $\mathbf{S}^c$
²⁸ deviatoric stress components are presented.

²⁹

³⁰ *2.3.1. The bond-stretching deviatoric stress component,* $\mathbf{S}^b$

³¹   As stated previously, the relaxation of $\mathbf{S}^b$ is a combination of elastic bond-stretching and
³² viscous flow of polymer segments. Figiel and Buckley [56] have shown that for kinematic
³³ structuring of constitutive models of finite deforming systems, an additive decomposition of
³⁴ elastic and viscous parts of the isochoric velocity gradients, $\overline{\boldsymbol{L}}$, is preferred to multiplicative
³⁵ decomposition of their deformation gradients. Also, Nemat-Nasser [57] has proposed that the
³⁶ deviatoric rate of deformation, $\overline{\mathbf{D}}$ can be additively decomposed into elastic, e and viscous,

1 v components for the whole polymer. In line with the latter assumption, the additive
2 decomposition of the total rate of deformation for the proposed model becomes:

$$\overline{\mathbf{D}} = \overline{\mathbf{D}}^e + \overline{\mathbf{D}}^v. \tag{6}$$

3 Since semicrystalline polymers show nonlinear viscoelastic behaviour, let us assume that
4 their rate of deformation can be described by linear elasticity and associative flow rule for
5 the elastic and viscous parts respectively. Therefore, the total deviatoric rate of deformation
6 becomes:

$$\overline{\mathbf{D}} = \overline{\mathbf{D}}^e + \overline{\mathbf{D}}^v \quad \longrightarrow \quad \overline{\mathbf{D}} = \frac{\hat{\mathbf{S}}_j^b}{2G_j^b} + \frac{\mathbf{S}_j^b}{\mu_j} \quad = \quad \frac{1}{2G_j^b}\left\{\hat{\mathbf{S}}_j^b + \frac{\mathbf{S}_j^b}{\tau_j}\right\} \tag{7}$$

7 where $j \in \{\alpha, \beta\}$ is the relevant viscoelastic relaxation process. The relaxation time, $\tau_j =$
8 $\frac{\mu_j}{2G_j^b}$ for the j−th process is defined in terms of a generalized stress-dependent viscosity, μ_j
9 and bond-stretching contribution to shear modulus, G_j^b. Also, $\hat{\mathbf{S}}_j^b$ is the Jaumann objective
10 rate [58] of the bond-stretching deviatoric stress. Therefore, for a given j-process, the
11 objective rate of $\mathbf{S}^b$ in the presence of a finite spin, $\mathbf{W}$ is expressed as *Equation 8*, where $\dot{\mathbf{S}}_j^b$
12 is the rate of change of Cauchy stress:

$$\hat{\mathbf{S}}_j^b = \dot{\mathbf{S}}_j^b - \mathbf{W}\mathbf{S}_j^b + \mathbf{S}_j^b\mathbf{W}. \tag{8}$$

13 For numerical predictions to fit experimental data accurately, each of the α- and β-
14 processes require a spectrum of relaxations times, τ_j, reflecting the range of molecular pack-
15 ing densities, and hence, activation barriers, where flow events occur in the polymer [12].
16 Let us define an N tensor-valued deviatoric stress state variable for a given process as $\mathbf{S}_{j,i}^b$
17 where $i = 1, 2, \ldots, N$. Employing a spectral generalization of *Equation 7*, the internal stress
18 at any instant can be expressed as:

$$\mathbf{S}_j^b = \sum_{i=1}^{N} \nu_{j,i}\mathbf{S}_{j,i}^b, \quad \hat{\mathbf{S}}_{j,i}^b = 2G_j^b\overline{\mathbf{D}} - \frac{\mathbf{S}_{j,i}^b}{\tau_{j,i}}, \quad \text{and} \quad \sum_{i=1}^{N} \nu_{j,i} = 1. \tag{9}$$

19 Here, $\nu_{j,i}(\tau_{j,i})$ is the normalized shear relaxation spectrum for a given j-process, at the in-
20 stant concerned. Assuming the spectrum to represent a range of activation barriers, the $\nu_{j,i}$
21 can be considered to be the volume fraction of the i−th barrier height for the j-process.
22
23 It has been shown by Wu and Buckley [12] that in the region of yield and post-yield
24 of polymer deformation, the full relaxation spectrum collapses into a single relaxation time
25 such that each α- or β-process corresponds to a geometric mean relaxation time i.e. τ_α and
26 τ_β. As proposed in the *GR model*, this relaxation time varies with: (a) temperature T, (b)
27 structure of the material as expressed through Tool's fictive temperature T_f, (c) mean stress,
28 σ_m and (d) octahedral shear stress, τ_{oct}. For a viscoelastic model based on the Eyring flow
29 process, the mean relaxation time, τ_j for $j \in \{\alpha, \beta\}$, can be related to its reference value,
30 $\tau_{j,0}^*$ in a stress-free reference configuration.
31
32 The resulting mean relaxation time for the j-process, under the effects of structure,
33 temperature and stress shift factors, for SCPs can be expressed as:

$$\tau_j = a_{T,j}a_{S,j}a_{\sigma,j}\tau_{j,0}^* \qquad \text{for} \quad j \in \{\alpha, \beta\}, \tag{10}$$

8

where $a_{T,j}$ = temperature shift factor, $a_{S,j}$ = structure shift factor and $a_{\sigma,j}$ = stress shift factor, for the j-process. Given the bond-stretching deviatoric stress component for the j-process as, $\mathbf{S}_j^b$, the octahedral shear stress formulation for this j-process is:

$$\tau_{\text{oct},j} = \sqrt{\frac{1}{3}\mathbf{S}_j^b : \mathbf{S}_j^b} \qquad \text{for} \quad j \in \{\alpha, \beta\}. \tag{11}$$

In the following, the formulations for the contributing shift factors in the context of the two-process constitutive model are presented.

Temperature Shift Factor, $a_{T,j}$: Temperature effects on the relaxation time are introduced through the Arrhenius equation, for the two j-processes, as:

$$a_{T,j} = \exp\left[\frac{\Delta H_j}{R}\left(\frac{1}{T} - \frac{1}{T^*}\right)\right], \qquad \text{for } j \in \{\alpha, \beta\}, \tag{12}$$

where ΔH_j represents the enthalpic contribution to the activation free energy barrier associated with the j-process, and T^* is a reference temperature.

Structure Shift Factor, $a_{S,j}$: The formulation of the structural shift factor for both processes is amenable to the similar fictive temperature description as the GR model, hence:

$$a_{S,j} = \exp\left[\frac{C}{T_{f,j} - T_\infty} - \frac{C}{T_{f,j}^* - T_\infty}\right], \quad \text{for} \quad j \in \{\alpha, \beta\}, \tag{13}$$

where C = Cohen-Turnbull constant; $T_{f,j}$ = fictive temperature for the j-process; and $T_{f,j}^*$ = corresponding reference fictive temperature; T_∞ is the Vogel temperature (where $\tau_j \to \infty$).

In order to incorporate the significant post-yield strain-softening observed in high rate compression of polypropylene [59], we adopt the relationship of structural evolution (through fictive temperature, T_f) with viscoplastic strain, strain rate and temperature, according to *Equation 14*. Accurate modeling of physical ageing requires a spectrum of T_f relaxation times. However, close to the glass transition, the following single mode representation was shown to be adequate by Lew and Buckley [60].

$$\dot{T}_{f,j} = \frac{T - T_{f,j}}{\tau_{S,j}} + \kappa D_j^v \qquad \text{for} \quad j \in \{\alpha, \beta\}. \tag{14}$$

Here κ is a material parameter, D_j^v is the invariant of the viscoplastic rate of deformation for the j-process, and $\tau_{S,j}$ is the corresponding structural relaxation time associated with the j-process (assumed here to have the same intrinsic value as the stress relaxation time and the same dependence on temperature and structure). The expressions for D_j^v and $\tau_{S,j}$ are:

$$D_j^v = \sqrt{\frac{1}{2}\mathbf{D}^v : \mathbf{D}^v} \quad \text{where} \quad \mathbf{D}^v = \overline{\mathbf{D}} - \frac{\hat{\mathbf{S}}_j^b}{2G_j^b} \quad \text{and} \quad \tau_{S,j} = a_{S,j}a_{T,j}\tau_{0,j}^*. \tag{15}$$

9

Stress Shift Factor, $a_{\sigma,j}$: The stress shift factor term of the relaxation spectrum results from the combined effects of the mean stress and the octahedral shear stress of the deforming polymer. This applies for each of the α- and β-processes. Using Eyring rate kinetics, the stress shift factor for the j-process can be expressed as [12]:

$$a_{\sigma,j} = \frac{\dfrac{V_{s,j}\tau_{oct,j}^{b}}{2RT}}{\exp\left\{\dfrac{V_{p,j}\sigma_m}{RT}\right\}\sinh\left\{\dfrac{V_{s,j}\tau_{oct,j}^{b}}{2RT}\right\}} \qquad \text{for} \quad j \in \{\alpha,\beta\} \tag{16}$$

where $V_{s,j}$ and $V_{p,j}$ are shear- and pressure-activation volumes respectively, for each of the processes.

The evolution of the stress shift factor term with relaxation times and the octahedral shear stress term of the polymer results in the presence of two dominant stress regimes, herein called the *high* and the *low stress regimes*. Simplified expressions of $a_{\sigma,j}$ for these regimes are given in *Equations 17* and *18*.

$$\left.a_{\sigma,j}\right|_{\text{high-stress}} = 2\frac{\tau_{\text{oct},j}^{b}}{\zeta_{0,j}}\exp\left[-\frac{\sigma_m}{\eta_{0,j}} - \frac{\tau_{\text{oct},j}^{b}}{\zeta_{0,j}}\right] \tag{17}$$

$$\left.a_{\sigma,j}\right|_{\text{low-stress}} = 2\frac{\tau_{\text{oct},j}^{b}}{\zeta_{0,j}}\left[\exp\left\{\frac{\tau_{\text{oct},j}^{b}}{\zeta_{0,j}}\right\} - \exp\left\{-\frac{\tau_{\text{oct},j}^{b}}{\zeta_{0,j}}\right\}\right]^{-1} \tag{18}$$

where $\zeta_{0,j}$ =shear-activation ratio and $\eta_{0,j}$ =pressure-activation (see *Equation C.1*). Detailed derivations and discussion of the stress shift factor term are given in *Appendix Appendix C*. These stress regimes and their corresponding simplified expresses of $a_{\sigma,j}$ will subsequently be used in deriving the Ree-Eyring yield function for the proposed constitutive model.

Combination of the $\alpha-$ and $\beta-$ stress components: The model has assumed that the bond-stretching deviatoric stress components from the two processes will combine independently leading to the total bond-stretching stress, $\mathbf{S}_{\text{Total}}^{b}$ of the model, thus:

$$\mathbf{S}_{\text{Total}}^{b} = \mathbf{S}_{\alpha}^{b} + \mathbf{S}_{\beta}^{b}, \tag{19}$$

where $\boldsymbol{S}_{\alpha}^{b}$ and $\boldsymbol{S}_{\beta}^{b}$ are the α- and β-process contributions to the deviatoric bond-stretching stress formulation. Similar approach of direct combination of the multi-process stress components for a semicrystalline polymer has been adopted by Caelers *et al.* [61, 62].

The summation defined above is also different from the approach adopted in composite-mechanics-type constitutive models for SCPs in which authors use the degree of crystallinity property as a means of partitioning contributions from the crystalline and other phases of

10

the semicrystalline polymer. In this work, we have assumed that such partition is redundant since the viscoelastic relaxations occur throughout the SCP microstructure albeit specific $\alpha-, \beta-$, or $\gamma-$ relaxations are more dominant in either of the mobile amorphous, crystalline or rigid amorphous fractions (consistent with evidence provided by Caelers *et al.* [61]). We also note that such assumption fits experimental data better.

2.4. The conformational deviatoric stress component, $\mathbf{S}^c$

Having established a formulation for the bond-stretching component, here we focus on the conformational stress component. The conformational statistics of the polymer macromolecules of the SCPs are defined using the isotropic hyper-elasticity proposed in the *GR model*. This accounts for the entropic elasticity of the polymer strands between entanglements as they stretch. It is assumed that a scalar free energy density function, A^c, exists which is used to derive the conformational stresses. In order to satisfy the requirement for objectivity, A^c must be independent of pure rotation, $\mathbf{R}$, hence A^c is determined uniquely by the deviatoric left stretch, $\overline{\mathbf{V}}$.

It is convenient to calculate the *conformational deviatoric stress component*, $\mathbf{S}^c$ directly by differentiating the conformational free energy density, A^c thus:

$$\mathbf{S}^c = \sum_{i}^{3} \overline{\lambda}_i \frac{\partial A^c}{\partial \overline{\lambda}_i} \mathbf{u}_i \otimes \mathbf{u}_i - p\boldsymbol{I} \qquad \text{where} \qquad p = \frac{1}{3}\text{trace}\left[\sum_{i}^{3} \overline{\lambda}_i \frac{\partial A^c}{\partial \overline{\lambda}_i} \mathbf{u}_i \otimes \mathbf{u}_i\right]. \qquad (20)$$

In *Equation 20*, $\overline{\lambda}_i$ $(i = 1, 2, 3)$ represents the eigenvalues of left stretch tensor, $\overline{\mathbf{V}}$, while $\mathbf{u}_i$ are the unit eigenvectors of $\overline{\mathbf{V}}$. The definition of the conformational entropy free energy function, A^c, is derived from the physically based function proposed by Edwards and Vilgis [63] for a network of cross-linked and entangled freely jointed chains of finite length[1].

The Edwards-Vilgis formulation of A^c is preferred over competing polymer network models as the Arruda-Boyce eight-chain model [64] and the Wu and van der Giessen full network model [65]. This is because Sweeney [66] has shown that the Edwards-Vilgis representation captures a broader range of material behaviour provided a finite extensibility of the chains is not approached too closely. For the purpose of a semicrystalline polymer here, the original Edwards-Vilgis formulation for A^c is reduced by assuming density of cross-links, $N_c = 0$ (true for thermoplastics), so that we obtain (ignoring cross-linking effect of crystals):

$$A^c = \frac{N_s k_B T}{2}\left[\frac{(1-\eta)(1-\alpha_n^2)}{1 - \alpha_n^2 \sum\limits_{i=1}^{3} \overline{\lambda}_i^2} \sum_{i=1}^{3} \frac{\overline{\lambda}_i^2}{1 + \overline{\lambda}_i^2} + \sum_{i=1}^{3} \ln\left(1 + \eta\overline{\lambda}_i^2\right) + \ln\left(1 - \alpha_n^2 \sum_{i=1}^{3} \overline{\lambda}_i^2\right)\right].$$

$$(21)$$

---

[1]Here, we have made the assumption that A^c applies to the whole polymer i.e. the $\alpha-$ and $\beta-$phases. It is not currently obvious that the $\alpha-$phase when fully relaxed would be rubber-elastic (since it is at least partially crystalline). We recognize therefore that this model is unlikely to be accurate at high temperatures or extremely long times, because of uncertainty about what the response of $\alpha-$phase would be under those conditions. However, because the relative contribution of $\boldsymbol{\sigma}^c$ is so small (see *Figure 9(c)*), under the conditions considered in the paper, the model predictions shown here are not sensitive to inaccuracy in it.

1 Here, N_s, α_n, η and k_B are respectively, the number density of *slip-links* (representing en-
2 tanglements), inextensibility of chains parameter, an index describing ease of entanglements
3 movement and Boltzmann's constant.
4

5 *2.5. Adiabatic heating considerations*

6 When polymers are subjected to impact/high strain rates of loading, a fraction of the
7 plastic work is converted into heat. The heat generated does not have time to transfer to
8 the surrounding, hence it is trapped within the material. This leads to thermal softening of
9 the test material. It is an example of *adiabatic heating*, and it has been found to be strain
10 and strain-rate dependent [67, 68, 69, 70]. For the proposed model to be applicable over a
11 wide range of dynamic loading, we incorporate a correction for the adiabatic heating.
12

13 For a polymer system subjected to dynamic loading, the instantaneous power balance
14 equation (assuming negligible kinetic energy) is given as:

$$\frac{\partial(\rho u)}{\partial t} = \boldsymbol{\sigma} : \mathbf{D} + \rho r - \boldsymbol{\nabla}(\mathbf{q}), \tag{22}$$

15 where ρ = density, u = specific internal energy, $\mathbf{q}$ = heat flux and r = specific internal power
16 source [11]. The power source term, r accounts for the *unrecoverable* additional energy stored
17 in bond-stretching due to structural change of the material, and r is expressed as:

$$r = -\Delta c \dot{T}_{fh}, \tag{23}$$

18 where Δc is the specific heat capacity step across the glass transition, and T_{fh} is the enthalpy
19 fictive temperature of the polymer system.
20

21 Neglecting any small changes in volume due to temperature rise and structural change
22 of the polymer, *Equation 22* for a single viscoelastic relaxation process system, becomes:

$$\rho c \dot{T} + \boldsymbol{\sigma}^b : \mathbf{D}^e = \boldsymbol{\sigma} : \mathbf{D} - \rho \Delta c \dot{T}_{fh}. \tag{24}$$

23 In order to evaluate, rate of change of the enthalpy fictive temperature, $\dot{T}_{fh}$ we have to un-
24 derstand the relationship between this value and the (structural change) mechanical fictive
25 temperature of *Equation 14* above. Buckley *et al.* [11] suggested that the two fictive tem-
26 perature measures are related thus: $\dot{T}_{fh} = \varphi \dot{T}_f$ where φ is a unknown material parameter.
27 Combining *Equations 14* and *24* yields a *single viscoelastic relaxation version* of the rate of
28 temperature rise under adiabatic heating conditions:

$$\dot{T}_{1-process} = \frac{1}{\rho c} \left[\boldsymbol{\sigma} : \mathbf{D} - \boldsymbol{\sigma}^b : \mathbf{D}^e \right] - \frac{\varphi \Delta c \dot{T}_f}{c}. \tag{25}$$

29 Extending *Equation 25* for a two viscoelastic relaxation version as the SCPs under con-
30 sideration here, we can re-write the equation as:

$$\dot{T}_{2-process} = \underbrace{\frac{1}{\rho c} \left[\boldsymbol{\sigma} : \mathbf{D} - \boldsymbol{\sigma}_\alpha^b : \mathbf{D}_\alpha^e - \boldsymbol{\sigma}_\beta^b : \mathbf{D}_\beta^e \right]}_{\text{plastic energy term}} - \underbrace{\frac{\varphi_\alpha \Delta c \dot{T}_{f,\alpha}}{c} - \frac{\varphi_\beta \Delta c \dot{T}_{f,\beta}}{c}}_{\text{structural rejuvenation term}}, \tag{26}$$

12

where $\varphi_j, \dot{T}_{f,j}$ and $\boldsymbol{\sigma}_j^b$ for $j \in \{\alpha, \beta\}$ in all cases, are respectively the material parameter, rate of change of fictive temperature and bond-stretching stress contributions of the j-processes. The applicable rate of deformation gradients are defined thus:

$$\mathbf{D}_\alpha^e = \mathbf{D} - \mathbf{D}_\alpha^v \implies \mathbf{D}_\alpha^e = \mathbf{D} - \frac{\boldsymbol{S}_\alpha^b}{2G_\alpha^b \tau_\alpha}, \text{ and} \tag{27}$$

$$\mathbf{D}_\beta^e = \mathbf{D} - \mathbf{D}_\beta^v \implies \mathbf{D}_\beta^e = \mathbf{D} - \frac{\boldsymbol{S}_\beta^b}{2G_\beta^b \tau_\beta}. \tag{28}$$

3. Application to experimental data

The proposed model will now be applied to experiments carried out on isotactic polypropylene (iPP). All model parameters were obtained from the results of many tests carried out on a grade of propathene polypropylene previously manufactured by ICI. Creep and tensile tests data reported by Okereke [71] were used to generate some of the model parameters. Also, compression tests data [59] generated across eight decades of strain rates, were used. Unlike the one-process *GR model*, the approach adopted here requires isolating the α- and β-process model parameters from linear viscoelasticity to post-yield regimes. For ease of reference, the data are presented in terms of *bond-stretching* and *conformational* model parameters.

3.0.1. Bond-stretching model parameters

The shear, G, and bulk, K, moduli were deduced from Young's modulus ($E = 1.8$ GPa, at quasi-static rates) and Poisson's ratio ($\nu = 0.43$)[72] during Hookean deformation in a tensile test, reported by Okereke [71]. The bulk modulus is introduced into the model via the total mean stress [10]:

$$\sigma_m = \left(K^b + K^c\right) \sum_{i=1}^{3} \epsilon_i, \tag{29}$$

where the bulk modulus, $K = K^b + K^c$, given that K^b and K^c are the bond-stretching and the conformational components of bulk moduli of the solid polymer. The conformation bulk modulus, K^c is quite small usually in order of magnitude (10^6 Pa) and when introduced into *Equation 29* will be dominated by the K^b value hence K^c is neglected when evaluating the total means stress, thus: $K \equiv K^b = E/[3(1 - 2\nu)] = 4.29$ GPa. Since the bulk modulus describes the hydrostatic response of the polymer, through the mean stress, σ_m, there was no need to distinguish between an $\alpha-$ and $\beta-$ process bulk moduli.

Similarly, for the shear modulus, $G^b \equiv G = E/2(1+v) = 0.6294$ GPa since $G^b \gg G^c$. Here, the G_α^b and G_β^b values were chosen to be both equal to the shear modulus, G of the bulk solid polymer. Consistent with the modelling philosophy proposed here, a priori, there should exist distinct values for both the $\alpha-$ and $\beta-$ bond-stretching shear moduli. This requires performing extensive dynamic mechanical analysis (DMA) tests to extract the temperature and time dependence of at least two independent elastic constants (shear modulus, bulk modulus, poison ratio, etc). Subsequently, contributions from the α and β relaxations

₁ would need to be decomposed from the resulting data. Unfortunately, the authors do not
₂ have these experimental data sets for polypropylene, or found any in published literature.
₃ We recognize that for completeness these tests need to be carried out, but at this stage of
₄ the work, we have not carried out this test. In lieu of this, we have carried out numerical
₅ simulations, and found that for the temperature window of the tests (at room temperature)
₆ the assumption of equal G^b values was sufficient to fit the experimental data well. A similar
₇ assumption was made by Mulliken *et al.* [7], where for Poisson ratio, ν, they assumed that
₈ $\nu_\alpha = \nu_\beta = \nu$. Also, the assumption of equal G^b for both $\alpha-$ and $\beta-$ processes was informed
₉ by the fact that the shear modulus in the temperature window of the compression data
₁₀ considered here, describes the solid state (small strains) deformation of the polymer hence:
₁₁ $G^b_\alpha = G^b_\beta = G$. In order to capture a wider range of temperatures, spanning the $\alpha-$ and $\beta-$
₁₂ viscoelastic relaxations, then a spectrum of relaxation times will have to be given, which
₁₃ consequently will lead to different shear moduli for $\alpha-$ and $\beta-$processes.

₁₅ The α- and β-processes activation enthalpies, (ΔH_α and ΔH_β) were obtained from creep
₁₆ tests reported by Okereke [71] and details of the derivations are given in *Appendix A*. The
₁₇ shear, $V_{s,j}$, and pressure, $V_{p,j}$, activation volumes for the j-processes were determined us-
₁₈ ing the compression data on polypropylene across a wide range of strain rates [59]. Eyring
₁₉ semi-log plots of σ_y/T versus true strain rates, $\dot{\lambda}/\lambda$, were plotted based on the compression
₂₀ test data. The yield stress, σ_y, was taken as the peak in true stress and λ is the uniaxial
₂₁ stretch at yield.

₂₃ For quasi-static response of the test polymer, and within the region of yield, the flow
₂₄ behaviour of the SCP is modelled using the Eyring rate kinetics formulation given thus:

$$\sigma_{y,j} = \frac{6RT}{\sqrt{2}V_{s,j} - 2V_{p,j}} \left[\ln(A_j) + \ln\left|\frac{\dot{\lambda}}{\lambda}\right| \right], \quad \text{for } A_j = \frac{\sqrt{2}G^b_j V_{s,j} a_{S,j} a_{T,j} \tau^*_{0,j}}{RT}, \quad (30)$$

₂₅ where τ^*_0 represents the reference relaxation time within the linear viscoelastic region. Recall
₂₆ that, $\tau^*_{0,j} = \dfrac{\mu^*_{0,j}}{2G^b_j}$ where $\mu^*_{0,j}$ is the j-process reference relaxation viscosity. Full derivations
₂₇ of *Equation 30* are given in *Appendix B*.

₂₉ The activation volume model parameters were determined based on the linear fits of the
₃₀ quasi-static and high-rate segments of the Eyring plot across the eight decades of time, as
₃₁ shown in *Figure 2*. The α-process slope, $M_{c,\alpha}$ is derived from linear fit of the low-rate seg-
₃₂ ment of the Eyring plot while the β-process slope, $M_{c,\beta}$ is obtained as the difference between
₃₃ the slopes of the linear fits of the low-rate and high-rate segments i.e. $M_{c,\beta} = M_{c,\alpha+\beta} - M_{c,\alpha}$.
₃₄ Here, the linear fit at high rate is represented as a combination of the α- and β- processes
₃₅ since at high rates both processes are known to dominate the flow response.

₃₇ The critical strain rate, $\dot{\epsilon}_{crit} = 10^{2.116} = 131 \text{ s}^{-1}$ represents the strain rate at which
₃₈ there is a significant change in slope of the Eyring plot, from the $\alpha-$process-dominant re-
₃₉ sponse to the combined $\alpha + \beta$ processes response. It is the basis used by some authors to
₄₀ describe the dependence of yield stress on strain rate as a *bilinear* response, for this type

14
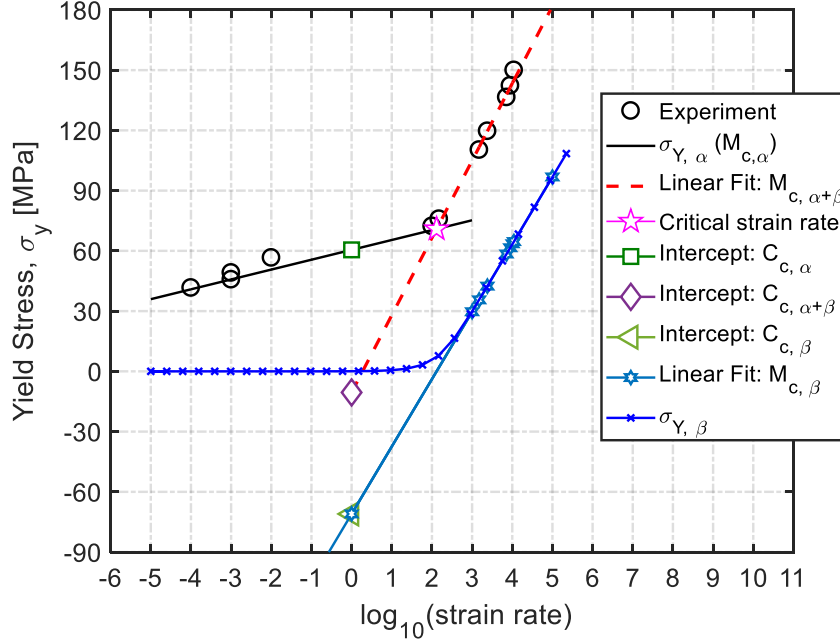
Figure 2: Eyring plot from compression test of iPP, showing slopes and intercept values for both α- and β-processes.

1 of material. In this work, we have shown that this is not necessarily a bilinear response
2 but a nonlinear response, whose mechanics is described by co-operative interactions of α-
3 and β-process dominant responses, described according to *Equations 30* and *36*, respectively.
4
5   Based on the Eyring rate kinetics formulation, it has been shown by Dooling *et al.* [55]
6 that the relationship between the activation volumes and the slopes data from an Eyring
7 plot is:

$$M_{c,j} = \frac{6R}{\sqrt{2}V_{s,j} - 2V_{p,j}} \quad , \text{ for } j \in \alpha, \beta \tag{31}$$

8 where $M_{c,j}$ is the slope of an Eyring plot of a compression test. These slopes were used to de-
9 termine the j-process apparent activation volume, $V_{app,j} = \frac{1}{3}\left(V_{s,j}\sqrt{2} - 2V_{p,j}\right)$, according to
10 *Equation 31*. The interdependence of $V_{s,j}$ and $V_{p,j}$ was based on the ratio: $V_{p,j}/V_{s,j} = 0.071$,
11 for polypropylene, which was obtained previously by Joseph and Duckett [73]. Using this
12 ratio, the activation volumes were determined and reported in *Table 1*.
13
14   The intercepts, C_j (for each j-process) of the linear fit of the Eyring plot were used to
15 determine the reference relaxation time, τ_0^*. Also, according to *Equation 32*, deduced as well
16 by Dooling *et al.* [55]:

$$\tau_{0,j}^* = \frac{\sqrt{2}RT}{2G^b V_{s,j}} \exp\left(\frac{C_{c,j}}{M_{c,j}}\right). \tag{32}$$

17 Using both $C_{c,j}$ and $M_{c,j}$ values of *Figure 2*, we obtained the reference relaxation times for
18 both α- and β-processes.
19

The glass transition temperature of the test polymer, $T_g = -3.2^oC$ (269.95 K)[74]. The compression test was carried out at room temperature, $T = 24.5^oC$ (297.65 K). The reference temperature, T^*, was chosen to be the test temperature, T, for compression test results of *Figures 4* to *7*. As a consequence, the two fictive temperatures are equal to the test temperature.

The rejuvenation parameter, κ_j, was found by matching the model prediction with the observed post-yield behaviour. The authors assumed that similar rejuvenation parameter applies for both α- and β-processes (i.e. $\kappa_\alpha = \kappa_\beta$). Further investigations need to be made to assess the suitability of this assumption. The Vogel limiting temperature, T_∞, and Cohen-Turnbull constant, C, were derived from the work on atactic polypropylene by Santangelo and co-workers [75] and the same parameters were assumed applicable for the tested iPP. This is the best data that is available to the authors but further improvements of the model should involve using more reliable values of C and T_∞[2].

3.0.2. Conformational model parameters

The entanglement molecular weight, M_e of the iPP was chosen based on the work of Eckstein and colleagues [76]. The authors considered the onset of plateau zone of a polypropylene melt to represent the rubbery network elasticity hence: $M_e = \dfrac{\rho RT}{G^0}$, where $G^0 = 0.427$ MPa is the plateau shear modulus. The experiment was carried out at $T = 190^oC$ and the density of iPP used in this work is $\rho = 907.8$ kg/m^3 such that we obtain $M_e = 8.1838$ kg/mol.

The model assumes an idealized rubbery network for capturing the conformational properties of the test polymer. Here, the polymer network is assumed to consist of several *tetra-functional* cross-links with physical entanglements. For the thermoplastic iPP under investigation, the entanglements/cross-links here were considered as *temporary junctions* called *slip links*. The number density of slip links, N_s for such network becomes [77]:

$$N_s = \frac{\rho N_A}{M_e} = 6.678 \times 10^{25} \text{ chains/m}^3 \tag{33}$$

where $N_A = 6.02 \times 10^{23}$ chains/mol is Avogadro's constant, and density, ρ, and entanglement molecular weight, M_e, are as described previously. The test polymer is temperature sensitive hence rubbery network entanglements will change with temperature. This implies that the mobility of the slip links of iPP will evolve from no sliding (solid) phase to a near perfect sliding (molten) phase. The condition of the polymer tested here is solid hence we assume a *slip link mobility factor, η* set to zero i.e. $\eta = 0$.

---

[2]Note that Santangelo and colleagues [75] obtained the C and T_∞ values by assuming that the temperature-dependence is informed solely by the Vogel-Tamman-Fulcher equation (*Equation 13*). However, in our proposed model (for an amorphous polymer in equilibrium), we assumed that some of the temperature-dependence comes from also an Arrhenius effect (see *Equation 12*). Therefore, we recognize that using the C and T_∞ above will predict too much temperature dependence.

Consider the unit cell of a body-centered monoclinic crystalline structure of iPP, where the typical physical dimensions of the unit cell are: $a = 6.65$Å, $c = 6.50$Å, and $b = 20.96$Å [78]. For this unit cell, there are 4 of chains, 12 monomer groups and 6 C-C pairs. Also, the bond length, L_b of a polypropylene molecule is $L_b = 1.544$Å [78] and the characteristic ratio, $C_\infty = 5.7$ [79]. Based on the unit cell, $\cos \psi = c/6L_b = 0.7016$ and number of bonds, $N_b = 2M^{-1}M_e = 390$ bonds, where M is the molar mass of a polypropylene monomer. Note that $\psi =$ the angle between the C-C bond and the c-axis of the polymer unit cell. Substituting these values into *Equation 34*, we determine the inextensibility factor, $\alpha_n = (1/\cos \psi)\sqrt{(C_\infty/N_b)} = 0.1723$, and the maximum stretch becomes: $\lambda_{max} = \alpha_n^{-1} = 5.8038$.

Under the effect of a stress tensor, the polymer network finite extensibility is set by the function, $\lambda_{max} \propto \sqrt{N}$ where λ_{max} is maximum stretch and N is the number of links in the polymer chain between junctions. The proposed model demands that we define a *network inextensibility factor,* α_n which defines the limit of this finite extensibility where $\lambda_{max} = 1/\alpha_n$. Here, the macromolecular configuration is also assumed to be represented by a *freely-jointed* virtual representation called a *Kuhn segment* which represents more than one chemical bond. For the iPP under investigation, the number of freely-jointed Kuhn segment, N_K is obtained thus:

$$N_K = \frac{\cos^2 \psi}{C_\infty}N_b \quad \equiv \quad N_K = \frac{1}{\alpha^2} \tag{34}$$

where ψ is the chemical bond angle, N_b is number of bonds and C_∞ is the characteristic ratio (usually greater than one) for the tested iPP.

Table 1 presents the set of model parameters for the *two-process model* for the major divisions of the model namely: *bond-stretching, conformational* and *adiabatic heating* parameters. References have been given for the source of model parameters that were not derived from experiments carried out by the authors. In the next section, we will explore the performance of the model as validation of its predictive fidelity.

4. Numerical implementation of the model

The model was implemented as a user-defined material model (UMAT) within the ABAQUS FE solver platform. An implicit version of the material sub-routine was developed and used for subsequent predictions of material responses reported in *Section 5*.

17

Table 1: Model parameters of polypropylene

Property/Parameter	Values	Source[3]
Bond-stretching stress terms		
Shear modulus , G [GPa]	0.510	[59]
Bulk Modulus, K [GPa]	3.71	
Poisson ratio, ν	0.43	[72]
Alpha activation enthalpy, ΔH_α [kJ/mol]	397	
Beta activation enthalpy, ΔH_β [kJ/mol]	236	[49]
Alpha shear activation volume, $V_{s,\alpha}$ [$\times 10^{-3}$ m^3/mol]	5.470	
Beta shear activation volume, $V_{s,\beta}$ [$\times 10^{-3}$ m^3/mol]	0.801	
Apparent activation volume ratio, $V_{p,j}/V_{s,j}$	0.071	[73]
Reference relaxation viscosity for α-process, $\mu_{0,\alpha}^*$ [Pa-s]	1.327×10^{12}	
Reference relaxation viscosity for β-process, $\mu_{0,\beta}^*$ [Pa-s]	6.235×10^{-2}	
Initial fictive temperature for j-process, $T_{f,j}^0$ [K]	297.65	
Reference fictive temperature for j-process, $T_{f,j}^*$ [K]	297.65	
Rejuvenation parameter for j-process, κ_j [Ks]	45.0	
Vogel limiting temperature, T_∞ [K]	234	[75]
Cohen-Turnbull constant, C [K]	1021	[75]
Reference temperature T^* [K]	297.65	
Conformational stress terms		
Density of slip links, N_s [atoms/mol]	6.678×10^{25}	
Network inextensibility factor, α_n	0.1723	
Slip link mobility factor, η	0	
Entanglement molecular weight, M_e [kg/mol] @ 463 K	8.184	[80]
Characteristic ratio, C_∞	5.7	[81]
Adiabatic heating terms		
Density, ρ [kg/m^3]	908	
Specific heat capacity, c [JK^{1}kg^1]	1667-1905	[82]
Effective specific heat difference for α-process, $\varphi_\alpha \Delta c_\alpha$ [J/kgK]	4000	
Effective specific heat difference for β-process, $\varphi_\beta \Delta c_\beta$ [J/kgK]	1000	

5. Discussions: *Performance of the model*

In this section, we assess the performance of the model by comparing model predictions to experimental data drawn from: (a) compression testing of polypropylene across a wide range of strain rates; and, (b) quasi-static tensile test of polypropylene across a range of temperatures from room temperature ($T = 25^oC$) to onset of flow ($T = 150^oC$). We will also provide further parametric studies of the *Two-process model* to assess the validity of model assumptions with respect to known experimental response for the class of polymer presented here.

---

[3]All values without references were either calculated or derived from experiments in this work.
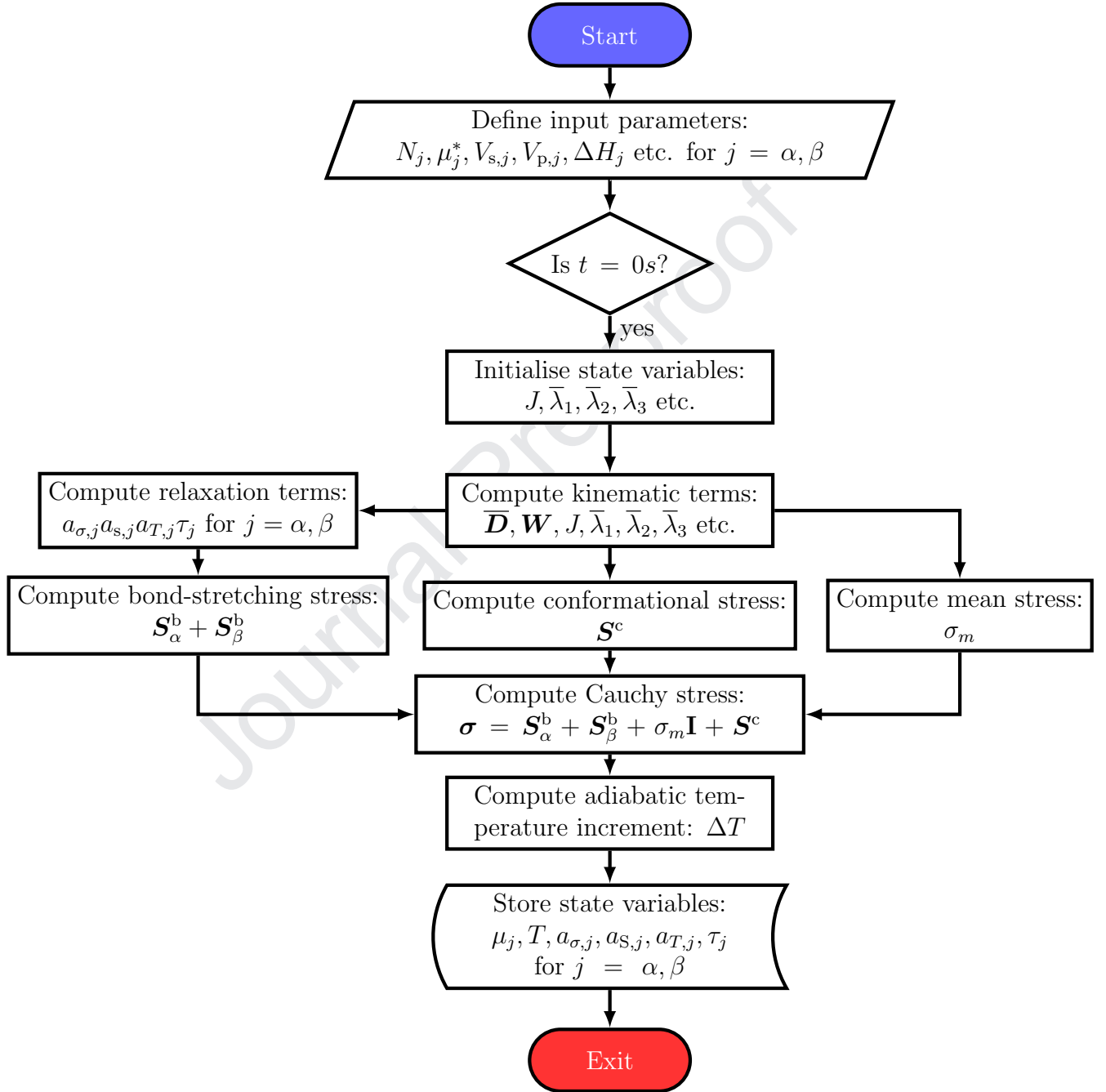
Figure 3: The model flow chart for the *Two-process model*.

5.1. Strain rate dependence

Compression test data were generated on a virgin homopolymer of polypropylene, and the experimental data for the ICIW grade of polypropylene has been reported by Okereke and co-workers [59]. The test data were generated across an unusual wide range of strain rates drawn from quasi-static (QS), to medium rate (MR) and high rate (HR) strain rates. The *Two-process model* was used to generate model predictions and the comparisons between model and experiment are shown in *Figure 4*. Note that the model as employed here is adiabatic, in order to capture response at the highest rates of deformation.
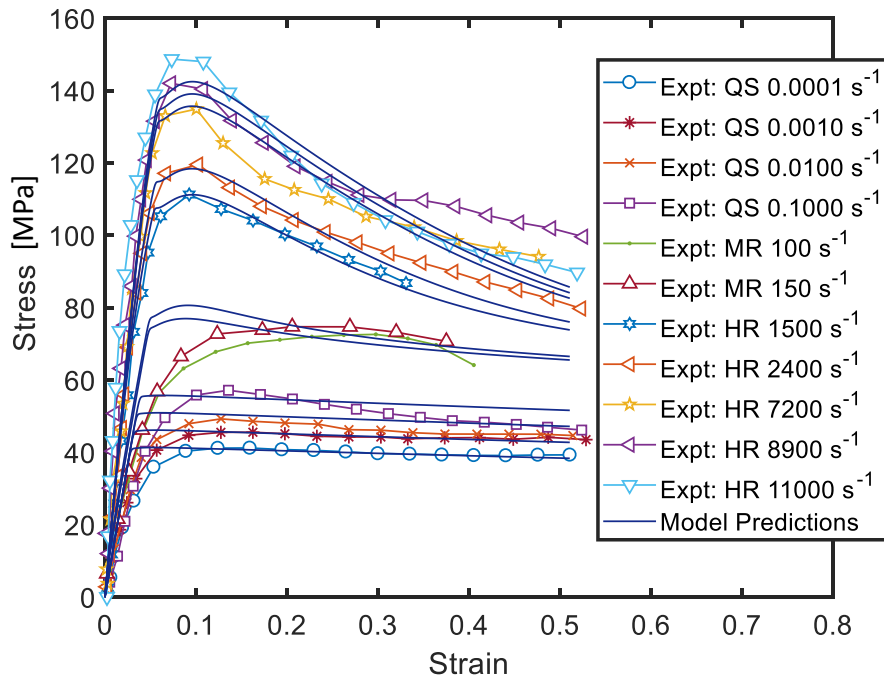
Figure 4: Comparison of experimental and model predictions for a compression test of an isotactic polypropylene test material. Test temperature is 25°C.

The experimental data reveal that with increasing strain rate, the Young's Modulus of the test material also increases. This trend is also captured by the model[4]. The yield and post-yield responses have also been reliably predicted using the model. However, shape of the region preceding yield is much sharper than the actual experimental data. This is because, in the current model prediction, the relaxation of the bond-stretching component of both $\alpha-$ and $\beta-$processes is far too localized in the time domain, as a result of use of a single relaxation time of the spring-dashpot. It is known that for quantitative fit to be achieved, especially in the region preceding yield, a spectrum of relaxation times should be used instead [10, 83]. Other authors have observed similar sharp pre-yield regions [7, 84, 85].

---

[4]For a reliable prediction of the rate-dependence of Young's Modulus as well as the exact shape of the yield region, the model need to incorporate a spectrum of relaxation times. Although the model formulation includes a spectrum of relaxation time (see *Equation 9*), the adjustment of model to experimental data has assumed a single relaxation time.

20

5.2. Rate-dependence of yield stress

The experimental data of *Figure 4* show the well-known feature of plastic deformation of polymeric solids: the pronounced rate-sensitivity of yield stress with increasing strain rate. Previously, in the model adjustment section, this rate-sensitivity, at moderate strain rates, was modelled according to the well-known Eyring theory of stress-biased thermal activation [86], and at small strain rates, the relationship between yield and strain rate is given in *Equation 30*.

There is literature evidence of nonlinear dependence of yield stress on strain rate (especially for the wide range of strain rates considered here). This is contradictory to classic Eyring theory [87, 88, 7], which describes a linear dependence. However, Bauwens has shown that the nonlinearity seen in PP data reported here, is consistent with the *two viscoelastic relaxation processes* contribution to the plastic flow, with activation volumes [87]. In such cases, the resulting plot of yield stress versus logarithm of strain rate is described as a *Ree-Eyring plot*, in honour of the seminal work of Ree and Eyring [89], who observed the influence of multiple processes to relaxation of condensed systems. The nonlinear Ree-Eyring plot of polypropylene, shown in *Figure 5*, is a consequence of the $\alpha-$ and $\beta-$processes, where each process has a corresponding activation volume (i.e. $V_{s,\alpha}$, $V_{s,\beta}$ for shear activation volumes and $V_{p,\alpha}$, $V_{p,\beta}$ for pressure activation volumes, of both processes).

Mathematically, we now re-define dependence of yield stress on strain rate in terms of the activation volumes for a multiple viscoelastic relaxation processes. We identify two dominant processes, which act co-operatively, to describe the total yield stress for a given strain rate. The first process, hereafter called *process 1*, is dominant at low strain rates and is described according to *Equation 30*. The second process, called *process 2*, is vanishingly small at low rates until the *critical strain rate*, $\dot{\epsilon}_{crit}$ is approached, beyond which it rises dramatically. At these quasi-static strain rate, the α contribution is dominant because the macromolecular response of the polymer is dominated by the restricted rotation and translation of the main chain within the crystalline region [7]. However, β is vanishingly small at quasi-static strain rates because the mobility of the polymer's side groups, in the amorphous region, is not significantly restricted. Beyond the critical strain rate threshold (or activation temperature), mobility of the side groups of the main chain in the amorphous zone become restricted, resulting in the manifestation of the secondary β relaxation.

The expressions of yield stress with respect to strain rate for both processes are described according to *Equations 35* and *36*. Detailed derivations of these two Ree-Eyring rate-dependent yield function (adapted for the proposed constitutive model) are given in *Appendix B* (see *Equations B.15* and *B.21*).

$$\sigma_{y,\alpha} = \frac{6RT}{V_{s,\alpha}\sqrt{2} - 2V_{p,\alpha}} \left[\ln|A_\alpha| + \ln\left(\frac{\dot{\lambda}}{\lambda}\right) \right] \tag{35}$$

$$\sigma_{y,\beta} = \frac{6RT}{\sqrt{2}V_{s,\beta}} \ln\left\{ \frac{A_\beta}{2}\frac{\dot{\lambda}}{\lambda} + \sqrt{\left(\frac{A_\beta}{2}\frac{\dot{\lambda}}{\lambda}\right)^2 + 1} \right\} \tag{36}$$

21

In these equations, R = gas constant, and T = temperature. A_j, (where $j \in \alpha, \beta$), is a material property defined in *Equation 30*; and $V_{s,j}$ and $V_{p,j}$ are respectively, the shear and pressure activation volumes for each $j-$ viscoelastic relaxation. The predicted total yield stress, resulting from the multiple processes, becomes:

$$\sigma_y = \sigma_{y,\alpha} + \sigma_{y,\beta} \tag{37}$$

Figure 5 shows the comparison between experimental yield data and model predictions according to the proposed *Two process model*. The results show a good fit between the two with the total yield stress identified as $\sigma_{y,\text{ Model predictions}}$, and results from *Equation 37*. In line with the underlying multiple-processes viscoelastic relaxation, the total yield stress results from a contribution of the $\alpha-$process dominant (process 1) and $\beta-$process dominant (process 2) viscoelastic relaxations. *Figure 5* also shows the linear relationship of process 1 according to *Equation 35* as well as the nonlinear relationship of process 2 (see *Equation 36*). We conclude here that the *Two process model* correctly predicts the dependence of yield stress on strain rate of polypropylene across the wide range of strain rate tested. As a result, the model will be useful for impact rates studies, as reported by Okereke *et al.* [90].
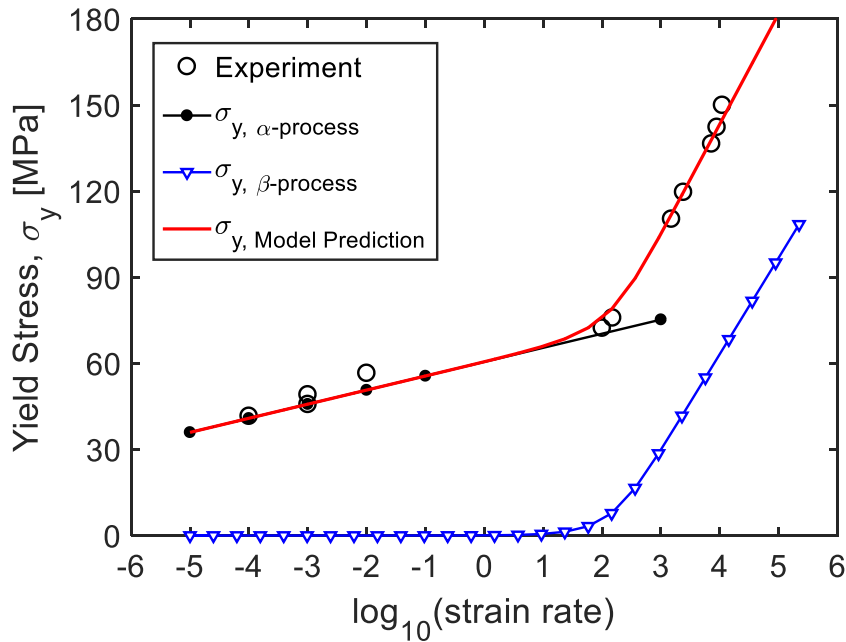
Figure 5: A Ree-Eyring plot of polypropylene test material at 25 ^{o}C. Plot shows the comparison model prediction and experimental data for the rate-dependent yielding of polypropylene. The plot also shows the linear $\alpha-$process plot and the nonlinear $\beta-$process.

5.3. Adiabatic heating effects

The *Two-process model* presented here exhibits *adiabatic heating effects*. To assess the effect of adiabatic heating to the compression test results, we undertook parametric studies

in which the adiabatic heating feature was switched off (see *Figure 6(a)*) and secondly, the adiabatic heating effect was included with the model prediction; however, the effect of structural change in adiabatic heating was switched off (see *Figure 6(b)*). Finally, both adiabatic heating and structural change effects were allowed to act cooperatively during the model prediction, as shown in *Figure 4*.
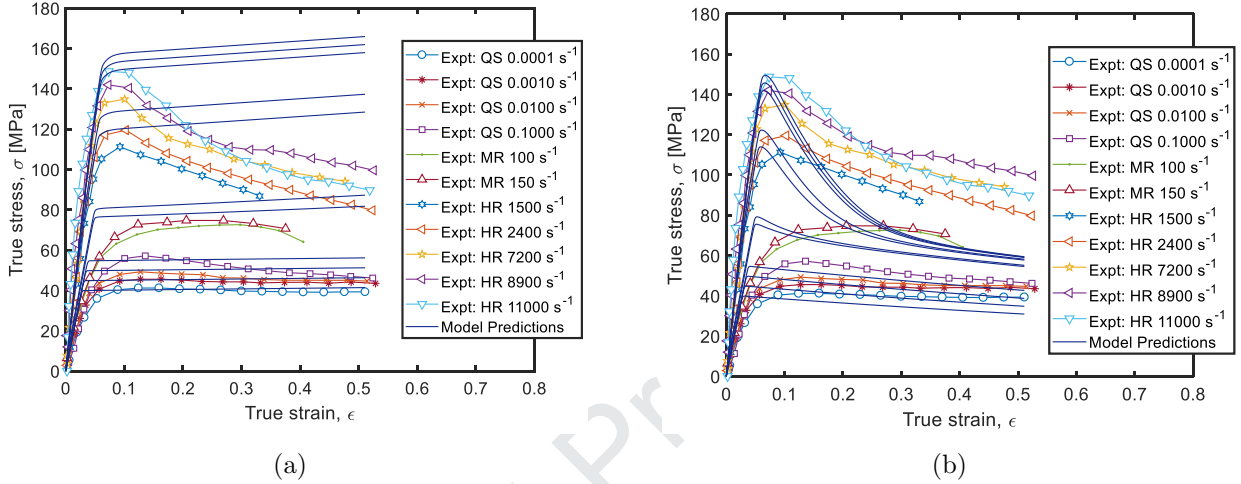
Figure 6: Comparison of experimental and model predictions for a polypropylene test material at 25 ^{o}C, showing: (a) no adiabatic heating effect and no structural effect and (b) adiabatic heating without structural effect.

Immediately, we notice that when adiabatic heating and structural change are excluded from the analysis (see *Figure 6(a)*), then the significant strain softening seen in high strain rates studies is not captured by the model. Again, if the implemented adiabatic heating formulation is included in model predictions (see *Figure 6(b)*), the model seems to over-predict when compared with experiments. As a result, too much adiabatic heat is flowing into the material leading to more strain softening than that seen in the experiment. Therefore, in line with *Equation 26*, we must also allow for structural change effects as well as adiabatic heating. The resulting prediction matches experiment as shown in *Figure 4*.

Finally, the evolution of adiabatic heating with respect to strain rate is shown in *Figure 7*. This shows that even at small strain rate of $\dot{\epsilon} = 0.001$ s^{-1}, there is a 10°C rise in temperature, because the model assumes perfect thermal insulation – i.e. adiabatic conditions. At the highest strain rate, $\dot{\epsilon} = 11000$ s^{-1}, the polypropylene experiences a 25° rise in temperature and this is entirely due to adiabatic heating effects. This is why it is essential to incorporate adiabatic heating formulation within any constitutive model required for predicting impact rates behaviour of such a material.

5.4. Temperature dependent effects

We show the effect of temperature dependence on the stress-strain profile, and the flow stress, σ_f, of the test polymer. The experimental data is compared with model predictions based on the *Two-process model*, and the results are given in *Figure 8*. These results are

23
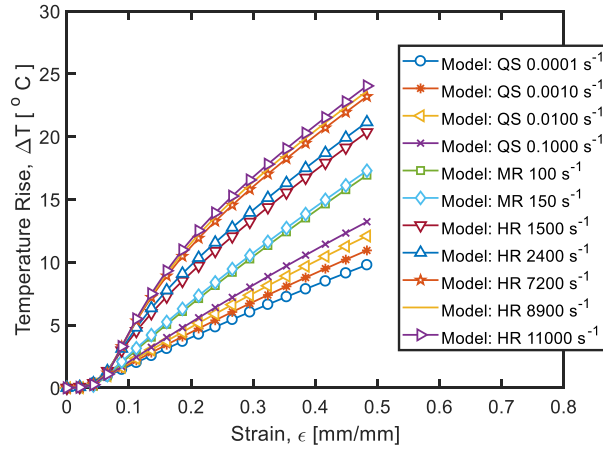
Figure 7: Model predictions of the strain-rate dependent evolution of adiabatic heating effects in the tested polypropylene material. Test temperature is 24.5^{o}C.

1 for quasi-static tests, with strain rate, $\dot{\epsilon} = 0.001$ s^{-1}, across a temperature, T range of
2 $30^{o}C \leq T \leq 150^{o}$. However, similar conclusions can be drawn when considering medium
3 and high rate tests, whilst accounting for the adiabatic heating and structural change effects
4 on the significant strain softening after yield.
5
6 The experimental data showed a brittle response at temperatures around room temper-
7 ature while at temperatures near the melting point of polypropylene (i.e. melting point,
8 $T_m = 165$ ^{o}C), a ductile response was observed. The flow stress, σ_f is the stress at which
9 thermal activation of the polymer macromolecular segments initiate a flow response. It is
10 herein chosen as the maximum stress on a given stress-strain graph. *Figure 8(b)* shows that
11 the proposed model captures this flow stress reliably, due to the Arrhenius function formu-
12 lation (see *Equation 12*) incorporated in the model's constitutive mathematics.
13
14 However, *Figure 8(a)* has revealed that in the region of small strains, the model did not
15 capture quantitatively the nonlinear plastic deformation. Experimental data show that with
16 increasing temperature, the Young's Modulus of the test material continues to decrease, due
17 to the softening of the polypropylene. Therefore, to quantitatively fit experiment to model,
18 we need to incorporate within the model a spectrum of relaxation times which spreads across
19 the solid-state (room-temperature) and flow-state (high-temperature) loading regimes. As
20 already argued for strain-rate dependent predictions, the choice here of a single relaxation
21 time for the model, is too localized in time domain, and this is evident in the poor fit within
22 the small strain predictions. Future improvements of the model should incorporate a spec-
23 trum of relaxation times for both quantitative and qualitative fit of the model to experiments.
24

25 *5.5. Interaction of the contributory stress components derived from the model*

26 In order to demonstrate the performance of the model in line with underlying assumption
27 of two-process formulation, we will now explore the multiple-process contributory stresses
28 that feed into the total stress prediction of the model. *Figure 9* shows the rate-dependent

24
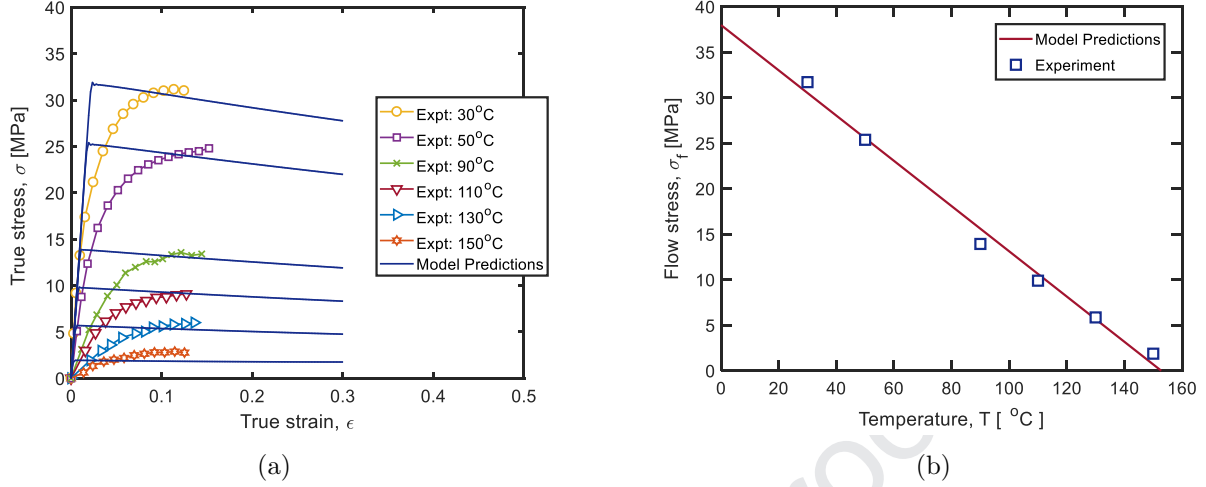
Figure 8: Temperature dependence effects for isotactic polypropylene showing comparison of experiments and model predictions for: (a) quasi-static uniaxial tensile test (for $\dot{\epsilon} = 0.001$ s^{-1}); and, (b) flow stress, σ_f (with flow stress identified as the maximum stress for a given stress-strain graph).

1 evolution of each of these contributory stresses (i.e. $\boldsymbol{S}^b_\alpha$, $\boldsymbol{S}^b_\beta$, $\boldsymbol{S}^c$, and $\boldsymbol{\sigma}_m$) across the range of
2 strain rates tested. *Figure 9(a)* shows that $\boldsymbol{S}^b_\alpha$ evolves with increasing strain rate with the
3 yield stress (maximum stress) spanning from 28 MPa at quasi-static strain rate, $\dot{\epsilon} = 0.0001$
4 s^{-1} to 57 MPa at high strain rate, $\dot{\epsilon} = 11,000$ s^{-1}. The influence of strain rate on yield stress
5 is much more dominant at the quasi-static rates while at the high strain rates, the difference
6 in the yield stresses is very minimal. Also, we notice that across the strain rates tested, the
7 Young's Modulus is independent of strain rate. This is in line with the model implementa-
8 tion of *Equation 7* where the shear modulus, G^b (which determines the Young's Modulus) is
9 specified as a rate-independent parameter. We can also observe that the maximum post-yield
10 strain softening across the strain rates, seen at $\dot{\epsilon} = 11,000$ s^{-1}, is $\Delta\sigma_{softening,\alpha} \approx 8$ MPa.
11 This suggests that the adiabatic heating and structural rejuvenation effects, that cause sig-
12 nificant post-yield strain softening, is minimal in $\boldsymbol{S}^b_\alpha$.
13
14 Also, *Figure 9(b)* shows that the β-process bond-stretching deviatoric stress, $\boldsymbol{S}^b_\beta$ are van-
15 ishingly small at quasi-static strain rates (see explanation in *Section 5.2*), but are dominant
16 at medium and high strain rates. This is consistent with model principle, which establishes
17 that in the low-strain rate (high temperature regime), the β-process deviatoric stress is in-
18 significant. This continues until the critical strain rate is reached, after which, there is a
19 sudden rise of the β-process stress (see *Figure 2* and *Equation 36*).
20
21 We also notice that in the immediate post-yield region of the β-stress curve, there is
22 a visible dip in the yield stress: a form of localized strain softening. This dip appears
23 at medium rates, but increases moderately with increasing strain rates. However, at the
24 highest strain rates, the dip just about vanishes. The authors investigated this by under-
25 taking parametric studies of the features of adiabatic heating and structural rejuvenation,
26 expected to influence the post-yield behaviour. The study revealed that the dip results from
27 a non-intuitive interaction between the adiabatic heating and structural rejuvenation effects.

25
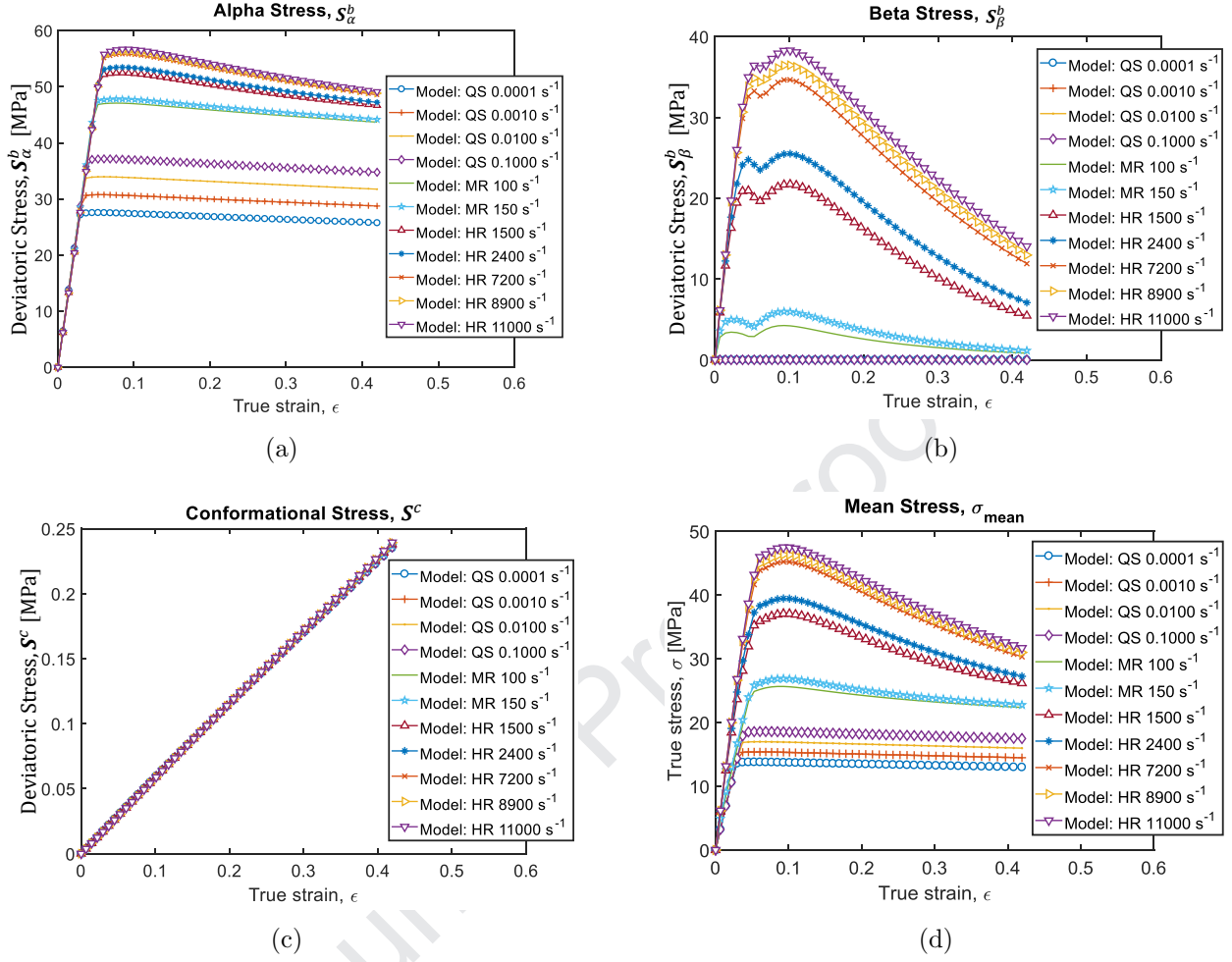
Figure 9: Effect on strain rates on the different contributory stresses, as predicted by the *Two-process model*, showing, bond-stretching deviatoric stresses for: (a) α-process, $\boldsymbol{S}_\alpha^b$, and (b) β-process, $\boldsymbol{S}_\beta^b$; as well as (c) conformational deviatoric stress, $\boldsymbol{S}_c$; and, (d) mean stress, σ_{mean}.

1 Initially, for medium rates, there was a sudden release of heat into the system arising from
2 adiabatic heating effects. As structural rejuvenation begins to dominate at higher strain
3 rates (~ 11000 s^{-1}), the adiabatic-heating-initiated dip is overwhelmed by structural reju-
4 venation effects and thus vanishes.
5
6 The β-process deviatoric stress, at strain rate, $\dot{\epsilon} = 11,000$ s^{-1}, also shows significant post-
7 yield strain softening, $\Delta\sigma_{softening,\beta} \approx 24$ MPa. This is three-times the strain softening due
8 to the α-process. This piece of evidence suggests that the $\beta-$process viscoelastic relaxation,
9 arising from the amorphous phase of the semicrystalline polymer, contributes significantly
10 to the adiabatic heating and structural rejuvenation effects: both processes that lead to
11 significant post-yield softening of the test polymer. Finally, we can also conclude that at
12 small strains, the contribution to modulus is rate-independent for both α- and β-stresses,
13 because both processes are approximated in the model as single relaxation time processes.
14

26

The plot of *Figure 9(c)* shows that the conformational deviatoric stress contribution to the model is quite minimal, with the highest stress at the highest strain rate being ~ 0.24 MPa. Within the strain rates, temperature and strain size of the experiments reported here for the polypropylene, the rubbery network effect of the polymer macromolecules is negligible. We also observe that the rubbery network effect is rate-independent.

Furthermore, *Figure 9(d)* shows the contribution of mean stress[5]. According to *Equation 4*, the predicted mean stress contribution is simply one-third of the stress shown in *Figure 4*. It plays a significant role in α- and β-processes via the pressure activation volumes. For example, at the highest strain rate, $\dot{\epsilon} = 11,000$ s^{-1}, the maximum mean stress is 47 MPa. This is significantly larger than the maximum stresses of the β-process and just lower than those of the α-process. The hydrostatic effect, based on the mean stress, contributes to the observed rate-dependence of Young's Modulus seen in the total stress prediction of *Figure 4*. This is in spite of the Young's Modulus, via the bond-stretching shear modulus, G^b, being a rate-independent quantity.

6. Conclusion

The constitutive modelling of semicrystalline polymers continues to prove a challenging task to material scientists. This is due in part to the multi-phasic, multi-component, hierarchical microstructure. As a result, several approaches have been used for modelling this type of polymer. In this work, we have proposed a constitutive model for semicrystalline polymers based on the underlying multi-process viscoelastic relaxations associated with the different phases that make up the polymer. The constitutive mathematics here represents a two-process extension of the *Glass-Rubber constitutive model*. Model predictions were compared with experimental data generated from compression tests on normal grade isotactic polypropylene across a wide range of strain rates (i.e. 10^{-4}s$^{-1} \leq \dot{\epsilon} \leq 10^4$ s^{-1}).

The model predictions have captured the major trends seen in the nonlinear viscoelastic responses of the chosen polymer namely: (a) rate-dependent yielding (b) temperature-dependence (c) adiabatic heating effects at high rates, and, (d) strain-induced rejuvenation. We have also shown the capability of the model to serve as a useful design and research tool in exploring the underlying rate-dependent relaxation processes that drive the constitutive behaviour of the semicrystalline polymer shown. The model can also be used to simulate semicrystalline polymers during solid-state processing at temperatures nearer the melting region, because it incorporates rubber-like entropic elasticity from the entangled molecular network, more prominent under those conditions. The model should serve as a significant analysis tool for design engineers, melt processing simulations as well as for academic research in the multi-process mechanics of the different phases of this type of semicrystalline polymer.

---

[5]The model has assumed that the contribution of conformation bulk modulus, K^c is negligible in comparison with the bond-stretching bulk modulus, K^b, which also dominates the overall bulk modulus, K (see *Equation 29*).

References

References

[1] McCrum, N., Buckley, C., Bucknall, C.. Principles of Polymer Engineering. Oxford science publications; Oxford University Press; 1997. ISBN 9780198565260. URL https://books.google.co.uk/books?id=UX-sAQAAQBAJ.

[2] Ward, I., Sweeney, J.. Mechanical Properties of Solid Polymers. Wiley; 2012. ISBN 9781119967118. URL https://books.google.co.uk/books?id=-sQNHQMYC1IC.

[3] Haward, R.. The Physics of Glassy Polymers. Springer Netherlands; 2012. ISBN 9789401158503. URL https://books.google.co.uk/books?id=lOvqCAAAQBAJ.

[4] Haward, R.N.. Strain hardening of thermoplastics. Macromolecules 1993;26(22):5860–5869.

[5] Haward, R.N.. The application of non-gaussian chain statistics to ultralow density polyethylenes and other thermoplastic elastomers. Polymer 1999;40(21):5821–5832.

[6] Boyce, M.C., Parks, D.M., Argon, A.S.. Large inelastic deformation of glassy polymers. part i: rate dependent constitutive model. Mechanics of Materials 1988;7(1):15–33.

[7] Mulliken, A.D., Boyce, M.C.. Mechanics of the rate-dependent elastic–plastic deformation of glassy polymers from low to high strain rates. International Journal of Solids and Structures, 2006;43(5):1331–1356.

[8] Dupaix, R.B., Boyce, M.C.. Constitutive modeling of the finite strain behavior of amorphous polymers in and above the glass transition. Mechanics of Materials 2007;39(1):39–52.

[9] Meijer, H.E.H., Govaert, L.E.. Mechanical performance of polymer systems: The relation between structure and properties. Progress in Polymer Science (Oxford) 2005;30(8-9):915–938.

[10] Buckley, C.P., Jones, D.C.. Glass-rubber constitutive model for amorphous polymers near the glass transition. Polymer 1995;36(17):3301–3312.

[11] Buckley, C.P., Dooling, P.J., Harding, J., Ruiz, C.. Deformation of thermosetting resins at impact rates of strain. part 2: Constitutive model with rejuvenation. Journal of the Mechanics and Physics of Solids 2004;52(10):2355–2377.

[12] Wu, J.J., Buckley, C.P.. Plastic deformation of glassy polystyrene: A unified model of yield and the role of chain length. Journal of Polymer Science, Part B: Polymer Physics 2004;42(11 SPEC. ISS.):2027–2040.

[13] Zia, Q., Mileva, D., Androsch, R.. Rigid amorphous fraction in isotactic polypropylene. Macromolecules 2008;41(21):8095–8102. doi:\bibinfo{doi}{10.1021/ma801455m}. http://dx.doi.org/10.1021/ma801455m; URL http://dx.doi.org/10.1021/ma801455m.

[14] Lu, Y., Men, Y.. Cavitation-Induced Stress Whitening in Semi-Crystalline Polymers. Macromolecular Materials and Engineering 2018;303(11):1800203. doi:\bibinfo{doi}{10.1002/mame.201800203}. URL https://onlinelibrary.wiley.com/doi/abs/10.1002/mame.201800203.

[15] Hay, I.L., Keller, A.. A study on orientation effects in polyethylene in the light of crystalline texture. Journal of Materials Science 1967;2(6):538–558. doi:\bibinfo{doi}{10.1007/BF00752220}. URL http://link.springer.com/10.1007/BF00752220.

[16] Peterlin, A.. Molecular model of drawing polyethylene and polypropylene. Journal of Materials Science 1971;6(6):490–508. doi:\bibinfo{doi}{10.1007/BF00550305}. URL http://link.springer.com/10.1007/BF00550305.

[17] Peterlin, A.. Plastic deformation of crystalline polymers. Polymer Engineering and Science 1977;17(3):183–193. doi:\bibinfo{doi}{10.1002/pen.760170307}. URL http://doi.wiley.com/10.1002/pen.760170307.

[18] Schultz, J.M.. Microstructural aspects of failure in semicrystalline polymers. Polymer Engineering and Science 1984;24(10):770–785. doi:\bibinfo{doi}{10.1002/pen.760241007}. URL http://doi.wiley.com/10.1002/pen.760241007.

[19] Galeski, A., Bartczak, Z., Argon, A.S., Cohen, R.E.. Morphological alterations during texture-producing plastic plane strain compression of high-density polyethylene. Macromolecules 1992;25(21):5705–5718. doi:\bibinfo{doi}{10.1021/ma00047a023}. URL https://pubs.acs.org/doi/abs/10.1021/ma00047a023.

[20] Bartczak, Z., Cohen, R.E., Argon, A.S.. Evolution of the crystalline texture of high-density polyethylene during uniaxial compression. Macromolecules 1992;25(18):4692–4704. doi:\bibinfo{doi}{10.1021/ma00044a034}. URL https://pubs.acs.org/doi/abs/10.1021/ma00044a034.

[21] G'sell, C., Dahoun, A.. Evolution of microstructure in semi-crystalline polymers under large plastic deformation. Materials Science and Engineering: A 1994;175(1-2):183–199. doi:\bibinfo{doi}{10.1016/0921-5093(94)91058-8}. URL https://www.sciencedirect.com/science/article/abs/pii/0921509394910588.

[22] Uchida, M., Tada, N.. Micro-, meso- to macroscopic modeling of deformation behavior of semicrystalline polymer. International Journal of Plasticity 2013;49:164 – 184. doi:\bibinfo{doi}{http://dx.doi.org/10.1016/j.ijplas.2013.03.007}. URL http://www.sciencedirect.com/science/article/pii/S0749641913000776.

[23] Caelers, H., Govaert, L., Peters, G.. The prediction of mechanical performance of isotactic polypropylene on the basis of processing conditions. Polymer 2016;83:116 – 128. doi:\bibinfo{doi}{http://dx.doi.org/10.1016/j.polymer.2015.12.001}. URL http://www.sciencedirect.com/science/article/pii/S0032386115304158.

[24] Oktay, H.E., Gürses, E.. Modeling of spherulite microstructures in semicrystalline polymers. Mechanics of Materials 2015;90:83 – 101. doi:\bibinfo{doi}{http://dx.doi.org/10.1016/j.mechmat.2015.04.010}. Proceedings of the {IUTAM} Symposium on Micromechanics of Defects in Solids; URL http://www.sciencedirect.com/science/article/pii/S0167663615001003.

[25] Li, X., Lin, Y., Ji, Y., Meng, L., Zhang, Q., Zhang, R., et al. Strain and temperature dependence of deformation mechanism of lamellar stacks in {HDPE} and its guidance on microporous membrane preparation. Polymer 2016;105:264 – 275. doi:\bibinfo{doi}{http://dx.doi.org/10.1016/j.polymer.2016.10.043}. Structure and Dynamics of Polymers studied by X-ray, Neutron and Muon Scattering; URL http://www.sciencedirect.com/science/article/pii/S0032386116309624.

[26] Sedighiamiri, A., Senden, D., Tranchida, D., Govaert, L., van Dommelen, J.. A micromechanical study on the deformation kinetics of oriented semicrystalline polymers. Computational Materials Science 2014;82:415 – 426. doi:\bibinfo{doi}{http://dx.doi.org/10.1016/j.commatsci.2013.09.068}. URL http://www.sciencedirect.com/science/article/pii/S0927025613006149.

[27] Brusselle-Dupend, N., Cangémi, L.. A two-phase model for the mechanical behaviour of semicrystalline polymers. part i: Large strains multiaxial validation on {HDPE}. Mechanics of Materials 2008;40(9):743 – 760. doi:\bibinfo{doi}{http://dx.doi.org/10.1016/j.mechmat.2008.03.011}. URL http://www.sciencedirect.com/science/article/pii/S0167663608000434.

[28] Ayoub, G., Zaïri, F., Naït-Abdelaziz, M., Gloaguen, J.. Modelling large deformation behaviour under loading–unloading of semicrystalline polymers: Application to a high density polyethylene. International Journal of Plasticity 2010;26(3):329 – 347. doi:\bibinfo{doi}{http://dx.doi.org/10.1016/j.ijplas.2009.07.005}. URL http://www.sciencedirect.com/science/article/pii/S0749641909000928.

[29] Epee, A., Lauro, F., Bennani, B., Bourel, B.. Constitutive model for a semi-crystalline polymer under dynamic loading. International Journal of Solids and Structures 2011;48(10):1590 – 1599. doi:\bibinfo{doi}{http://dx.doi.org/10.1016/j.ijsolstr.2011.02.009}. URL http://www.sciencedirect.com/science/article/pii/S0020768311000680.

[30] Senden, D., Peters, G., Govaert, L., Dommelen, J.V.. Anisotropic yielding of injection molded polyethylene: Experiments and modeling. Polymer 2013;54(21):5899 – 5908. doi:\bibinfo{doi}{http://dx.doi.org/10.1016/j.polymer.2013.08.047}. URL http://www.sciencedirect.com/science/article/pii/S0032386113008306.

[31] Maurel-Pantel, A., Baquet, E., Bikard, J., Bouvard, J., Billon, N.. A thermo-mechanical large deformation constitutive model for polymers based on material network description: Application to a semi-crystalline polyamide 66. International Journal of Plasticity 2015;67:102 – 126. doi:\bibinfo{doi}{http://dx.doi.org/10.1016/j.ijplas.2014.10.004}. URL http://www.sciencedirect.com/science/article/pii/S0749641914001983.

[32] Garcia-Gonzalez, D., Zaera, R., Arias, A.. A hyperelastic-thermoviscoplastic constitutive model for semi-crystalline polymers: Application to {PEEK} under dynamic loading conditions. International Journal of Plasticity 2016;:–doi:\bibinfo{doi}{http://dx.doi.org/10.1016/j.ijplas.2016.09.011}. URL http://www.sciencedirect.com/science/article/pii/S0749641916301760.

[33] Bardenhagen, S.G., Stout, M.G., Gray, G.T.. Three-dimensional, finite deformation, viscoplastic

1   constitutive models for polymeric materials. Mechanics of Materials 1997;25(4):235–253.

2 [34] Hasanpour, K., Ziaei-Rad, S.. Finite stain viscoelastic-plastic deformation of polymers using finite
3   element simulation. AIP Conference Proceedings 2007;908:1301–1306.

4 [35] Hong, K., Rastogi, A., Strobl, G.. A model treating tensile deformation of semicrystalline poly-
5   mers: Quasi-static stress-strain relationship and viscous stress determined for a sample of polyethylene.
6   Macromolecules 2004;37(26):10165–10173.

7 [36] Hong, K., Rastogi, A., Strobl, G.. Model treatment of tensile deformation of semicrystalline polymers:
8   Static elastic moduli and creep parameters derived for a sample of polyethylene. Macromolecules
9   2004;37(26):10174–10179.

10 [37] Men, Y., Rieger, J., Strobl, G.. Role of the Entangled Amorphous Network in Tensile Deformation
11   of Semicrystalline Polymers. Physical Review Letters 2003;91(9):095502. doi:\bibinfo{doi}{10.1103/
12   PhysRevLett.91.095502}. URL https://link.aps.org/doi/10.1103/PhysRevLett.91.095502.

13 [38] Song, Y., Nemoto, N.. Application of an interpenetrating network model to the solid deformation
14   of a quenched isotactic polypropylene film. Polymer 2005;46(17):6522–6530. doi:\bibinfo{doi}{10.
15   1016/J.POLYMER.2005.05.058}. URL https://www.sciencedirect.com/science/article/pii/
16   S0032386105006208.

17 [39] Song, Y., Koh-hei Nitta, ,, , Nemoto, N.. Molecular Orientations and True Stress-Strain Relationship
18   in Isotactic Polypropylene Film 2003;doi:\bibinfo{doi}{10.1021/MA030194D}. URL https://pubs.
19   acs.org/doi/abs/10.1021/ma030194d.

20 [40] Keith, H.D., Padden, F.J., Vadimsky, R.G.. Intercrystalline Links: Critical Evaluation. Journal
21   of Applied Physics 1971;42(12):4585–4592. doi:\bibinfo{doi}{10.1063/1.1659827}. URL http://aip.
22   scitation.org/doi/10.1063/1.1659827.

23 [41] Nitta, K., Takayanagi, M.. Role of tie molecules in the yielding deformation of isotactic polypro-
24   pylene. Journal of Polymer Science Part B: Polymer Physics 1999;37(4):357–368. doi:\bibinfo{doi}
25   {10.1002/(SICI)1099-0488(19990215)37:4⟨357::AID-POLB9⟩3.0.CO;2-I}. URL https://doi.org/10.
26   1002/(SICI)1099-0488(19990215)37:4<357::AID-POLB9>3.0.CO;2-I.

27 [42] Jourdan, C., Cavaille, J.Y., Perez, J.. Mechanical relaxations in polypropylene: A new experimental
28   and theoretical approach. Journal of Polymer Science Part B: Polymer Physics 1989;27(11):2361–
29   2384. doi:\bibinfo{doi}{10.1002/polb.1989.090271115}. URL http://dx.doi.org/10.1002/polb.
30   1989.090271115.

31 [43] Buckley, C.P., McCrum, N.G.. Anisotropy of the mechanical α-relaxation in biaxially oriented linear
32   polyethylene. Journal of Materials Science 1973;8(7):928–940. doi:\bibinfo{doi}{10.1007/BF00756623}.
33   URL https://doi.org/10.1007/BF00756623.

34 [44] Boyd, R.H.. Relaxation processes in crystalline polymers: molecular interpretation - a review. Polymer
35   1985;26(8):1123–1133.

36 [45] Schawe, J.E.K.. Mobile amorphous, rigid amorphous and crystalline fractions in isotactic polypro-
37   pylene during fast cooling. Journal of Thermal Analysis and Calorimetry 2017;127(1):931–937. doi:
38   \bibinfo{doi}{10.1007/s10973-016-5533-4}. URL https://doi.org/10.1007/s10973-016-5533-4.

39 [46] Sweeney, J., Spares, R., Woodhead, M.. A constitutive model for large multiaxial deformations of
40   solid polypropylene at high temperature. Polymer Engineering and Science 2009;49(10):1902–1908.

41 [47] Suljovrujic, E., Trifunovic, S., Milicevic, D.. The influence of gamma radiation on the dielectric re-
42   laxation behaviour of isotactic polypropylene: The relaxation. Polymer Degradation and Stability
43   2010;95(2):164 – 171. doi:\bibinfo{doi}{http://dx.doi.org/10.1016/j.polymdegradstab.2009.11.034}.
44   URL http://www.sciencedirect.com/science/article/pii/S014139100900384X.

45 [48] Hoyos, M., Tiemblo, P., Gómez-Elvira, J.M.. Influence of microstructure and semi-crystalline mor-
46   phology on the and mechanical relaxations of the metallocene isotactic polypropylene. European Poly-
47   mer Journal 2009;45(4):1322 – 1327. doi:\bibinfo{doi}{http://dx.doi.org/10.1016/j.eurpolymj.2009.01.
48   018}. URL http://www.sciencedirect.com/science/article/pii/S0014305709000111.

49 [49] McCrum, N.G.. Kinetics of the alpha and beta relaxations in isotactic polypropylene. Polymer
50   1984;25(3):299–308.

51 [50] McCrum, N., Read, B., Williams, G.. Anelastic and Dielectric Effects in Polymeric Solids. Dover
52   Books on Engineering; Dover Publications; 1967. ISBN 9780486667522. URL https://books.google.
53   co.uk/books?id=x1zBQgAACAAJ.

54 [51] Bauwens-Crowet, C.. Compression yield behaviour of polymethyl methacrylate over a wide range of

temperatures and strain-rates. Journal of Materials Science 1973;8(7):968–979.

[52] Brusselle-Dupend, N., Cangémi, L.. A two-phase model for the mechanical behaviour of semicrystalline polymers. part {II} – modelling of the time-dependent mechanical behaviour of an isotropic and a highly oriented {HDPE} grade. Mechanics of Materials 2008;40(9):761 – 770. doi:\bibinfo{doi}{http://dx. doi.org/10.1016/j.mechmat.2008.03.010}. URL http://www.sciencedirect.com/science/article/pii/S016766360800046X.

[53] Okereke, M., Keates, S.. Material Response: Measures of Stress and Strain. Cham: Springer International Publishing. ISBN 978-3-319-67125-3; 2018, p. 299–362. doi:\bibinfo{doi}{10.1007/978-3-319-67125-3_9}. URL https://doi.org/10.1007/978-3-319-67125-3_9.

[54] Buckley, C.P., Jones, D.C., Jones, D.P.. Hot-drawing of poly(ethylene terephthalate) under biaxial stress: Application of a three-dimensional glass-rubber constitutive model. Polymer 1996;37(12):2403–2414.

[55] Dooling, P.J., Buckley, C.P., Rostami, S., Zahlan, N.. Hot-drawing of poly(methyl methacrylate) and simulation using a glass - rubber constitutive model. Polymer 2002;43(8):2451–2465.

[56] Figiel, L., Buckley, C.P.. On the modelling of highly elastic flows of amorphous thermoplastics. International Journal of Non-Linear Mechanics 2009;44(4):389 – 395. doi:\bibinfo{doi}{http://dx.doi.org/10.1016/j.ijnonlinmec.2009.01.005}. URL http://www.sciencedirect.com/science/article/pii/S0020746209000158.

[57] Nemat-Nasser, S.. Decomposition of strain measures and their rates in finite deformation elasto-plasticity. International Journal of Solids and Structures 1979;15(2):155–166. doi:\bibinfo{doi}{10.1016/0020-7683(79)90019-2}. URL https://www.sciencedirect.com/science/article/pii/0020768379900192.

[58] Holzapfel, G.. Nonlinear Solid Mechanics: A Continuum Approach for Engineering. Wiley; 2000. ISBN 9780471823193. URL https://books.google.co.uk/books?id=_ZkeAQAAIAAJ.

[59] Okereke, M.I., Buckley, C.P., Siviour, C.R.. Compression of polypropylene across a wide range of strain rates. Mechanics of Time-Dependent Materials 2012;16(4):361–379. doi:\bibinfo{doi}{10.1007/s11043-012-9167-z}. URL http://dx.doi.org/10.1007/s11043-012-9167-z.

[60] Lew, A.C.Y., Buckley, C.P.. Improved glass-rubber constitutive model for biaxial hot drawing of amorphous poly(ethylene terephthalate). In: 23rd annual meeting of the polymer processing society, Salvador, Brazil. 2007,.

[61] Caelers, H., Govaert, L., Peters, G.. The prediction of mechanical performance of isotactic polypropylene on the basis of processing conditions. Polymer 2016;83:116 – 128. doi:\bibinfo{doi}{https://doi.org/10.1016/j.polymer.2015.12.001}. URL http://www.sciencedirect.com/science/article/pii/S0032386115304158.

[62] M., C.H.J., Emanuele, P., Dario, C., M., P.G.W., E., G.L.. Deformation and failure kinetics of ipp polymorphs. Journal of Polymer Science Part B: Polymer Physics ????;55(9):729–747. doi:\bibinfo{doi}{10.1002/polb.24325}. https://onlinelibrary.wiley.com/doi/pdf/10.1002/polb.24325; URL https://onlinelibrary.wiley.com/doi/abs/10.1002/polb.24325.

[63] Edwards, S., Vilgis, T.. The effect of entanglements in rubber elasticity. Polymer 1986;27(4):483 – 492. doi:\bibinfo{doi}{http://dx.doi.org/10.1016/0032-3861(86)90231-4}. URL http://www.sciencedirect.com/science/article/pii/0032386186902314.

[64] Arruda, E.M., Boyce, M.C.. A three-dimensional constitutive model for the large stretch behavior of rubber elastic materials. Journal of the Mechanics and Physics of Solids 1993;41(2):389 – 412. doi:\bibinfo{doi}{http://dx.doi.org/10.1016/0022-5096(93)90013-6}. URL http://www.sciencedirect.com/science/article/pii/0022509693900136.

[65] Wu, P., Giessen, E.V.D.. On improved network models for rubber elasticity and their applications to orientation hardening in glassy polymers. Journal of the Mechanics and Physics of Solids 1993;41(3):427 – 456. doi:\bibinfo{doi}{http://dx.doi.org/10.1016/0022-5096(93)90043-F}. URL http://www.sciencedirect.com/science/article/pii/002250969390043F.

[66] Sweeney, J.. A comparison of three polymer network models in current use. Computational and Theoretical Polymer Science 1999;9(1):27 – 33. doi:\bibinfo{doi}{http://dx.doi.org/10.1016/S1089-3156(98)00050-6}. URL http://www.sciencedirect.com/science/article/pii/S1089315698000506.

[67] Mason, J., Rosakis, A., Ravichandran, G.. On the strain and strain rate dependence of the fraction of plastic work converted to heat: an experimental study using high speed infrared detectors

31

and the kolsky bar. Mechanics of Materials 1994;17(2):135 – 145. doi:\bibinfo{doi}{http://dx.doi.org/10.1016/0167-6636(94)90054-X}. URL http://www.sciencedirect.com/science/article/pii/016766369490054X.

[68] Rittel, D.. On the conversion of plastic work to heat during high strain rate deformation of glassy polymers. Mechanics of Materials 1999;31(2):131 – 139. doi:\bibinfo{doi}{http://dx.doi.org/10.1016/S0167-6636(98)00063-5}. URL http://www.sciencedirect.com/science/article/pii/S0167663698000635.

[69] Safari, K.H., Zamani, J., Guedes, R.M., Ferreira, F.J.. The effect of heat developed during high strain rate deformation on the constitutive modeling of amorphous polymers. Mechanics of Time-Dependent Materials 2016;20(1):45–64. doi:\bibinfo{doi}{10.1007/s11043-015-9283-7}. URL http://dx.doi.org/10.1007/s11043-015-9283-7.

[70] Torres, J., Frontini, P.. Mechanics of polycarbonate in biaxial impact loading. International Journal of Solids and Structures 2016;85–86:125 – 133. doi:\bibinfo{doi}{http://dx.doi.org/10.1016/j.ijsolstr.2016.02.010}. URL http://www.sciencedirect.com/science/article/pii/S0020768316000640.

[71] Okereke, M.I.. Prediction of finite deformation of themoplastic matrix composites. Ph.D. thesis; Oxford University; 2009.

[72] Okereke, M., Akpoyomare, A.. A virtual framework for prediction of full-field elastic response of unidirectional composites. Computational Materials Science 2013;70:82 – 99. doi:\bibinfo{doi}{http://dx.doi.org/10.1016/j.commatsci.2012.12.036}. URL http://www.sciencedirect.com/science/article/pii/S0927025612007744.

[73] Joseph, S., Duckett, R.. Effects of pressure on the non-linear viscoelastic behaviour of polymers: 1. polypropylene. Polymer 1978;19(7):837 – 843. doi:\bibinfo{doi}{http://dx.doi.org/10.1016/0032-3861(78)90014-9}. URL http://www.sciencedirect.com/science/article/pii/0032386178900149.

[74] Bai, F., Li, F., Calhoun, B.H., Quirky, R.P., Chen, S.Z.D.. Physical Constants of Poly(propylene). Polymer Handbook; Hoboken, New Jersey: Wiley-Interscience; 4th ed.; 1999, p. V/21–V/30.

[75] Santangelo, P., Ngai, K., Roland, C.. Temperature dependence of relaxation in polypropylene and poly (ethylene-co-propylene). Macromolecules 1996;29(10):3651–3653.

[76] Eckstein, A., Suhm, J., Friedrich, C., Maier, R.D., Sassmannshausen, J., Bochmann, M., et al. ????;.

[77] Treloar, L.. The Physics of Rubber Elasticity. Monographs on the physics and chemistry of materials; Oxford University Press, USA; 1975. ISBN 9780191523304. URL https://books.google.co.uk/books?id=EfCZXXKQ50wC.

[78] Bai, F., Li, F., Calhoun, B.H., Quirky, R.P., Chen, S.Z.D.. Physical Constants of Poly(propylene). Polymer Handbook; Hoboken, New Jersey: Wiley-Interscience; 4th ed.; 1999, p. V/21–V/30.

[79] Suter, U.W., Flory, P.J.. Conformational energy and configurational statistics of polypropylene. Macromolecules 1975;8(6):765–776. doi:\bibinfo{doi}{10.1021/ma60048a018}. http://dx.doi.org/10.1021/ma60048a018; URL http://dx.doi.org/10.1021/ma60048a018.

[80] Eckstein, A., Suhm, J., Friedrich, C., Maier, R.D., Sassmannshausen, J., Bochmann, M., et al. Determination of plateau moduli and entanglement molecular weights of isotactic, syndiotactic, and atactic polypropylenes synthesized with metallocene catalysts. Macromolecules 1998;31(4):1335–1340.

[81] Flory, P., Jackson, J.. Statistical Mechanics of Chain Molecules. Hanser; 1989. ISBN 9781569900192. URL https://books.google.co.uk/books?id=NJxTPgAACAAJ.

[82] Gaur, U., Wunderlich, B.. Heat capacity and other thermodynamic properties of linear macromolecules. iv. polypropylene. Journal of Physical and Chemical Reference Data 1981;10(4).

[83] Ferry, J.. Viscoelastic Properties of Polymers. Wiley; 1980. ISBN 9780471048947. URL https://books.google.co.uk/books?id=9dqQY3Ujsx4C.

[84] van Breemen, L., Govaert, L., Meijer, H.. Scratching polycarbonate: A quantitative model. Wear 2012;274:238 – 247. doi:\bibinfo{doi}{http://dx.doi.org/10.1016/j.wear.2011.09.002}. URL http://www.sciencedirect.com/science/article/pii/S0043164811005849.

[85] van Breemen, L., Klompen, E., Govaert, L., Meijer, H.. Extending the egp constitutive model for polymer glasses to multiple relaxation times. Journal of the Mechanics and Physics of Solids 2011;59(10):2191 – 2207. doi:\bibinfo{doi}{http://dx.doi.org/10.1016/j.jmps.2011.05.001}. URL http://www.sciencedirect.com/science/article/pii/S0022509611000925.

32

[86] Eyring, H.. Viscosity, plasticity, and diffusion as examples of absolute reaction rates. The Journal of chemical physics 1936;4(4):283–291.

[87] Bauwens, J.C.. Relation between the compression yield stress and the mechanical loss peak of bisphenol-a-polycarbonate in the β transition range. Journal of Materials Science 1972;7(5):577–584. doi:\bibinfo{doi}{10.1007/BF00761956}. URL https://doi.org/10.1007/BF00761956.

[88] Chou, S.C., Robertson, K.D., Rainey, J.H.. The effect of strain rate and heat developed during deformation on the stress-strain curve of plastics. Experimental Mechanics 1973;13(10):422–432.

[89] Ree, F., Ree, T., Eyring, H.. Relaxation theory of transport problems in condensed systems. Industrial & Engineering Chemistry 1958;50(7):1036–1040.

[90] Okereke, M.I., Le, C.H., Buckley, C.P.. A new constitutive model for prediction of impact rates response of polypropylene. In: DYMAT2012 - 10th International DYMAT Conference. EPJ Web of Conferences; 2012,.

[91] Boyd, R.H.. Relaxation processes in crystalline polymers: experimental behaviour - a review. Polymer 1985;26(3):323–347.

Appendix A. Activation Enthalpy, $\Delta H_{0,j}^a$ of the Arrhenius Equation

According to the formulation of the proposed model, temperature-dependence is introduced into the model formulation from a combined effect of an Arrhenius-style effect and a structural-evolution effect due to fictive temperature. As part of the adjusting of the model to experimental data, we have used creep test results carried out within the α-relaxation temperature range from which $\Delta H_{0,\alpha}$ was determined for the polypropylene grade used in this work. We need to extract the Arrhenius-style-only activation enthalpy from the creep test data, without the influence of structural-evolution-only effect.

In line with the model formulation, the time-dependent shift factor, $a_{t,j}$ used in constructing a creep master curve is a combined effect of structure, $a_{S,j}$ and Arrhenius-effect shift factors, $a_{T,j}$ for a given j-process. Hence:

$$a_{t,j} = a_{S,j}a_{T,j} \quad \Rightarrow \quad \ln a_{t,j} = \ln a_{S,j} + \ln a_{T,j}. \tag{A.1}$$

Taking the derivative of both sides with respect to the reciprocal of temperature:

$$\frac{d\ln a_{t,j}}{d\left(\frac{1}{T}\right)} = \frac{d\ln a_{S,j}}{d\left(\frac{1}{T}\right)} + \frac{d\ln a_{T,j}}{d\left(\frac{1}{T}\right)} \implies m_{t,j} = m_{S,j} + m_{T,j}, \tag{A.2}$$

where the m-terms are the slopes of plots of shift factors against inverse of temperature. We can obtain the $m_{t,j}$-term from a typical creep test where temperature is varied as shown in *Figure A.10*. The $m_{S,j}$-term can be obtained by taking the logarithmic expression for the Vogel-Talman-Fulcher formulation of a j-process shown in *Equation 13* and the result becomes:

$$\ln a_{S,j} = \left[\frac{C}{T_f - T_\infty} - \frac{C}{T_f^* - T_\infty}\right] \tag{A.3}$$

where C, T_f, T_f^*, T_∞ are material constants defined in *Table 1* for the tested polymer. Taking the derivative of *Equation A.3* with respective to $\frac{1}{T_f}$ becomes:

$$\frac{d\ln a_{S,j}}{d\left(\frac{1}{T_f}\right)} = \frac{CT_f^2}{(T_f - T_\infty)^2} \tag{A.4}$$

Finally, the $m_{T,j}$-term can likewise be derived by evaluating the derivative with respect to inverse of temperature of the natural logarithm of *Equation 12*.

$$\ln a_{T,j} = \frac{\Delta H_{0,j}}{R}\left[\frac{1}{T} - \frac{1}{T^*}\right] \tag{A.5}$$

where $\Delta H_{0,j}$ is the temperature-only enthalpic contribution to the activation free energy barrier of the j-process. *Equation A.5* is a linear plot of $\ln a_{T,j}$ with respect to inverse of temperature. The linear plot will have a slope:

$$m_{T,j} = \frac{d(R\ln a_{T,j})}{d\left(\frac{1}{T}\right)} \implies m_{T,j} = \Delta H_{0,j}. \tag{A.6}$$

The value of $\Delta H_{0,j}$ can therefore be determined based on *Equations A.2* and *A.4* thus:

$$m_{j,T} = m_{t,j} - m_{t,S} \quad \implies \quad \Delta H_{0,j} = m_{t,j} - \left(\frac{CT_f^2}{(T_f - T_\infty)^2} \right). \tag{A.7}$$

Appendix A.1. Determination of α-process activation enthalpy,$\Delta H_{0,\alpha}$

For the polypropylene grade tested in creep in this work, a typical creep compliance plot is shown in *Figure 10(a)* and the resulting Arrhenius function plot of same data following a time-temperature shifting (to generate a master curve) is given in *Figure 10(b)*. Since the temperature range in which the creep test was undertaken was in the α-viscoelastic relaxation range $20^0\text{C} \leq T \leq 100^0\text{C}$, the applicable process is $j = \alpha$ [91].
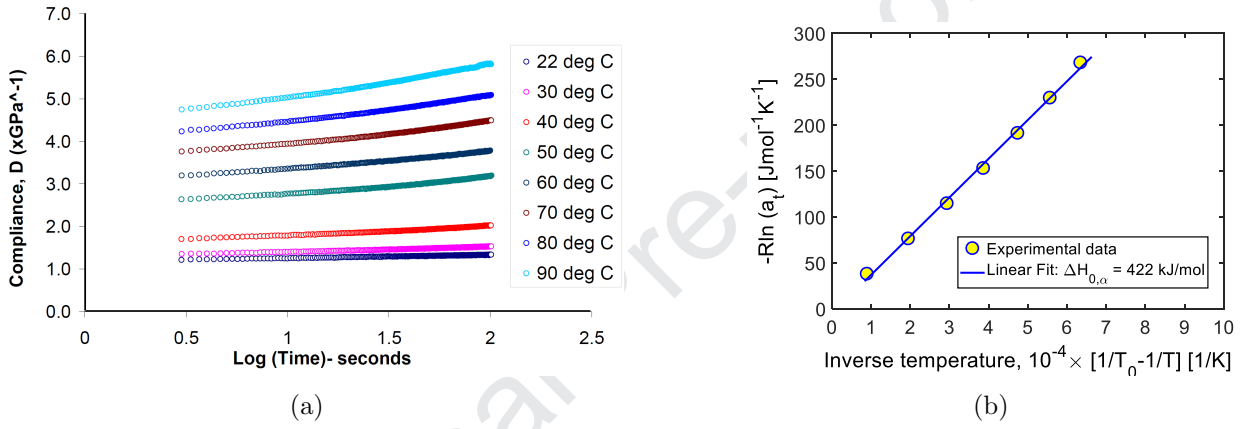
Figure A.10: Creep test results of iPP tested across varying temperature showing: (a) Creep compliance plot and (b) Arrhenius function plot where a_t is the time-dependent shift factor, R is the gas constant, and $T_0 = 20^0\text{C}$ is the reference (ambient) temperature.

The slope of the creep curve $m_{t,\alpha} = 422$ kJ/mol, and this is equal to $\Delta H_{0,\alpha}$ (note $\Delta H_{0,\alpha}=$ overall activation enthalpy incorporating both structural and temperature relaxation effects). Parameters for the structural shift factor, $a_{S,j}$ equation were obtained from the work on atactic polypropylene by Santangelo and co-workers [75] in which they determined the following material constants[6] of the Vogel-Tamman-Fulcher equation: $C = 1021$, $T_\infty = 233.5$K. Same values will be used for the polymer under investigation here. In adjusting model to experimental data (see *Section 3*), we assumed that the polypropylene is in structural equilibrium hence $T = T_f$. Similarly, for evaluating the activation enthalpy for the α-process, we assume also that the fictive temperature in *Equation A.8*, to be equal to the current test temperature for each creep test. Hence, we can now evaluate the temperature-only activation enthalpy for the tested polypropylene thus:

$$\begin{aligned} \Delta H_{0,\alpha} &= m_{t,\alpha} - \frac{CT_f^2}{(T_f - T_\infty)^2} \\ &= 4.22 \times 10^5 - \frac{1021 \times 293.15^2}{(293.15 - 233.5)^2} = 3.9734 \times 10^5 \text{ J/mol} \\ \Delta H_{0,\alpha} &= 397 \text{ kJ/mol}. \end{aligned} \tag{A.8}$$

---

[6]See footnote 2, on the implication of use of these VTF constants in our proposed model.

1 *Appendix A.2. Determination of β-process temperature-only activation enthalpy,$\Delta H_{0,\beta,T}$*

2   In the β-viscoelastic relaxation range for isotactic polypropylene, the applicable temper-
3 ature range is: $-40^0\mathrm{C} \leq T \leq 0^0\mathrm{C}$ [91]. We will need to carry out viscoelastic tests (like
4 creep or stress relaxation) within this temperature range to determine the β-process activa-
5 tion enthalpy. Since the authors did not carry out such tests, we use the results of McCrum
6 [49] based on polypropylene. McCrum used a process he described as *thermal sampling* to
7 determine different activations values based on two test methods for temperature range of
8 $-16.1^o\mathrm{C} \leq T \leq -27.3^o\mathrm{C}$. Since the peak on a $\tan\delta$ versus temperature, T plot of polypro-
9 pylene is at about $-10^o\mathrm{C}$, we therefore choose the activation energy values closest to this
10 i.e. $T = -16.1^o\mathrm{C}$. Therefore the activation enthalpy for the β-process becomes:

$$\Delta H_{0,\beta,T} = 56.4 \text{ kcal/mol} \implies \Delta H_{0,\beta,T} = 236 \text{ kJ/mol}. \tag{A.9}$$

Appendix B. Derivations of Ree-Eyring rate-dependent yield formulations

In order to compare model predictions with compression test data from Okereke *et al.* [59], we need to derive the Ree-Eyring yield functions for such a compression test. Consider a typical cylindrical specimen with three bases vectors (e_i, for $i = 1, 2, 3$), as shown in *Figure B.11*.
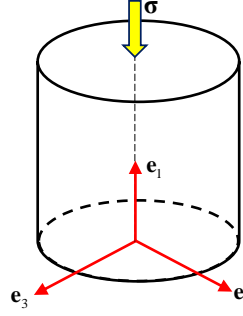
Figure B.11: A schematic diagram of a compression test specimen, subjected to a stress tensor, $\boldsymbol{\sigma}$.

The specimen is subjected to a stress tensor, $\boldsymbol{\sigma}$ which results in a strain tensor, $\boldsymbol{\epsilon}$ and strain rate, $\dot{\boldsymbol{\epsilon}}$. For such a uniaxial compression specimen, $\sigma_{11} = \sigma$, $\sigma_{22} = \sigma_{33} = 0$ and $\tau_{12} = \tau_{23} = \tau_{13} = 0$, where σ is the magnitude of the uniaxial compressive load imposed on the specimen. Therefore, the mapping expressions between material (x_i) and spatial (X_i) coordinate systems, are given as:

$$x_1 = X_1(1 - \dot{\epsilon}t) \tag{B.1}$$
$$x_2 = X_2(1 + \dot{\epsilon}t) \tag{B.2}$$
$$x_3 = X_3(1 + \dot{\epsilon}t) \tag{B.3}$$

The deformation gradient tensor, $\boldsymbol{F}$ and the rate of change of deformation gradient, $\dot{\boldsymbol{F}}$, can be expressed thus:

$$\boldsymbol{F} = \frac{\partial \boldsymbol{x}}{\partial \boldsymbol{X}} = \begin{bmatrix} 1 - \dot{\epsilon}t & 0 & 0 \\ 0 & 1 + \dot{\epsilon}t & 0 \\ 0 & 0 & 1 + \dot{\epsilon}t \end{bmatrix} \quad \text{and} \quad \dot{\boldsymbol{F}} = \frac{\partial \boldsymbol{x}}{\partial t} = \begin{bmatrix} -\dot{\epsilon} & 0 & 0 \\ 0 & \dot{\epsilon} & 0 \\ 0 & 0 & \dot{\epsilon} \end{bmatrix} \tag{B.4}$$

Therefore, the volume ratio, J, becomes:

$$J = \det \boldsymbol{F} = \left(1 - \epsilon t\right)\left(1 + \epsilon t\right)^2 \tag{B.5}$$

Using J, we describe expressions for deviatoric deformation gradient, $\bar{\boldsymbol{F}}$, the velocity gradient tensor, $\bar{\boldsymbol{F}}$, and deviatoric rate of deformation gradient, $\bar{\boldsymbol{D}}$ become:

$$\bar{\boldsymbol{F}} = J^{-\frac{1}{3}}\boldsymbol{F}, \qquad \bar{\boldsymbol{L}} = \dot{\boldsymbol{F}}\boldsymbol{F}^{-1}, \quad \text{and} \quad \bar{\boldsymbol{D}} = \tfrac{1}{2}\left(\bar{\boldsymbol{L}} + \bar{\boldsymbol{L}}^T\right) \tag{B.6}$$

1 Let us also define the stress tensor, $\boldsymbol{\sigma}$ for a uniaxial compression test and the mean/hydrostatic
2 stress thus:

$$\boldsymbol{\sigma} = \begin{bmatrix} \sigma & 0 & 0 \\ 0 & 0 & 0 \\ 0 & 0 & 0 \end{bmatrix} \quad \text{and} \quad \sigma_m = \text{tr}(\boldsymbol{\sigma}) = \tfrac{1}{3}\sigma \tag{B.7}$$

3 Hence the deviatoric stress tensor, $\bar{\boldsymbol{S}}$, for a uniaxial compression test defined by *Equation*
4 *B.7* becomes:

$$\bar{\boldsymbol{S}} = \boldsymbol{\sigma} - \sigma_m \boldsymbol{I} \quad \longrightarrow \quad \bar{\boldsymbol{S}} = \begin{bmatrix} \tfrac{2}{3}\sigma & 0 & 0 \\ 0 & -\tfrac{1}{3}\sigma & 0 \\ 0 & 0 & -\tfrac{1}{3}\sigma \end{bmatrix} \tag{B.8}$$

5 Material reference objectivity is introduced to the *Two-process model* by converting the
6 bond-stretching form of the deviatoric stress tensor into its Jaumann objective rate form, $\hat{\boldsymbol{S}}^b$,
7 in accordance with *Equation 8*, defined previously. For the compression test under consider-
8 ation, the spin $\boldsymbol{W} = 0$, hence $\hat{\boldsymbol{S}}^b = \dot{\boldsymbol{S}}_j^b$, where $\dot{\boldsymbol{S}}_j^b$ is the rate of change of the bond-stretching
9 Cauchy stress tensor, for a $j-$process.
10

11 Also, in the region of yield, $\dot{\boldsymbol{S}}_j^b = 0$ and $\boldsymbol{S}_j^c = 0$, such that based on *Equation 9*, without
12 the spectral generalization (i.e. no relaxation spectrum), we obtain:

$$\hat{\boldsymbol{S}}_j^b = 2G_j^b \bar{\boldsymbol{D}} - \frac{\boldsymbol{S}_j^b}{\tau_j} \quad \longrightarrow \quad \boldsymbol{S}_j^b = 2G_j^b \bar{\boldsymbol{D}} \tau_j = \boldsymbol{S} \quad \text{since} \quad \hat{\boldsymbol{S}}^b = \dot{\boldsymbol{S}}_j^b = 0 \tag{B.9}$$

13 *Equation B.9* is the desired constitutive equation that has to be solved and implemented
14 for the compression test under investigation. Through the relaxation time, τ_j, the nonlin-
15 ear viscoelasticity associated with the polymer response is introduced into the constitutive
16 equation. The τ_j term is dependent on the stress shift factor of *Equation 16*. We will now
17 expand the constitutive equation for the specific cases of high or low stress regimes.

18 • **Case A: Compression at yield for the high stress regime**: In this regime,
19   we will re-define the constitutive equation of *Equation B.9*, especially in the region
20   around yield for the compression test specimen.
21

22   For the compression test specimen, and as shown previously: $\boldsymbol{\sigma}(1,1) = \sigma$, $\boldsymbol{S}_j^b(1,1) =$
23   $\boldsymbol{S}(1,1) = \tfrac{2}{3}\sigma$, and, the rate of change of deformation gradient, $\bar{\boldsymbol{D}} = \dot{\epsilon}_{11}$ where $\dot{\epsilon}_{11}$ is the
24   dominant strain rate of the compression test, and 1 is test direction is the test direction
25   (see *Figure B.11*) . Applying these and *Equation 10*, to the constitutive equation of
26   *Equation B.9*, for only the $1-$axis test direction yields:

$$\begin{aligned} \boldsymbol{S}_j^b &= 2G_j^b \tau_j \bar{\boldsymbol{D}} \\ \tfrac{2}{3}\sigma_j &= 2G_j^b \tau_j \left| \dot{\epsilon}_{11} \right| \\ \tfrac{2}{3}\sigma_j &= 2G_j^b a_{S,j} a_{T,j} a_{\sigma,j} \tau_{0,j}^* \left| \dot{\epsilon}_{11} \right| \end{aligned}$$

Substituting the expression for the high stress regime shift factor (see *Equation C.5*) into the above becomes:

$$\frac{2}{3}\sigma_j \;=\; 2\left\{ 2\frac{\tau_{\text{oct},j}^b}{\zeta_{0,j}} \exp\left[-\frac{\sigma_m}{\eta_{0,j}} - \frac{\tau_{\text{oct},j}^b}{\zeta_{0,j}} \right] \right\} G_j^b a_{S,j} a_{T,j} \tau_{0,j}^* \left|\dot{\epsilon}_{11}\right| \tag{B.10}$$

However, the bond-stretching octahedral shear stress, τ_{oct}^b can be expressed in terms of the uniaxial stress, σ for the compression test as:

$$\tau_{oct,j}^b = \sqrt{\tfrac{1}{3}\boldsymbol{S}_j^b : \bar{\boldsymbol{S}}_j^b} = \sqrt{\tfrac{1}{3}\bar{\boldsymbol{S}} : \bar{\boldsymbol{S}}} \quad \longrightarrow \quad \tau_{oct,j}^b = \frac{\sqrt{2}}{3}\sigma \tag{B.11}$$

Applying *Equation B.11* into *Equation B.10* results in:

$$\frac{2}{3}\sigma_j \;=\; 2\left\{ 2\left(\frac{\sqrt{2}}{3}\frac{\sigma_j}{\zeta_{0,j}} \right) \exp\left[-\frac{\sigma_m}{\eta_{0,j}} - \frac{\sqrt{2}}{3}\frac{\sigma_j}{\zeta_{0,j}} \right] \right\} G_j^b a_{S,j} a_{T,j} \tau_{0,j}^* \left|\dot{\epsilon}_{11}\right|$$

$$1 \;=\; \exp\left[-\frac{\sigma_m}{\eta_{0,j}} - \frac{\sqrt{2}}{3}\frac{\sigma_j}{\zeta_{0,j}} \right] \frac{2\sqrt{2}G_j^b a_{S,j} a_{T,j} \tau_{0,j}^*}{\zeta_{0,j}} \left|\dot{\epsilon}_{11}\right|$$

Re-arranging the equation:

$$\exp\left[\frac{\sigma_m}{\eta_{0,j}} + \frac{\sqrt{2}}{3}\frac{\sigma_j}{\zeta_{0,j}} \right] \;=\; \frac{2\sqrt{2}G_j^b a_{S,j} a_{T,j} \tau_{0,j}^*}{\zeta_{0,j}} \left|\dot{\epsilon}_{11}\right|$$

Taking the natural log of both sides gives:

$$\frac{\sigma_m}{\eta_{0,j}} + \frac{\sqrt{2}}{3}\frac{\sigma_j}{\zeta_{0,j}} \;=\; \ln\left[\frac{2\sqrt{2}G_j^b a_{S,j} a_{T,j} \tau_{0,j}^*}{\zeta_{0,j}} \right] + \ln\left|\dot{\epsilon}_{11}\right|$$

Multiply across by $\zeta_{0,j}$, thus we obtain:

$$\sigma_m \frac{\zeta_{0,j}}{\eta_{0,j}} + \frac{\sqrt{2}}{3}\sigma_j = \zeta_{0,j}\ln\left[\frac{2\sqrt{2}G_j^b a_{S,j} a_{T,j} \tau_{0,j}^*}{\zeta_{0,j}} \right] + \zeta_{0,j}\ln\left|\dot{\epsilon}_{11}\right|$$

Note that in the region around yield, $\sigma_{m,j} = -\frac{1}{3}\sigma_{y,j}$ where $\sigma_{y,j}$ is the yield stress for the $j-$process. Also, note that all stress measures become equal to the yield stress i.e. $\sigma_j \equiv \sigma_{y,j}$ in the region of yield. Using these, we obtain:

$$\left[\sqrt{2} - \frac{\zeta_{0,j}}{\eta_{0,j}} \right]\sigma_{y,j} \;=\; 3\zeta_{0,j}\ln\left[\frac{2\sqrt{2}G_j^b a_{S,j} a_{T,j} \tau_{0,j}^*}{\zeta_{0,j}} \right] + 3\zeta_{0,j}\ln\left|\dot{\epsilon}_{11}\right|$$

39

Finally, we make $\sigma_{y,j}$ the subject of the formula:

$$\sigma_{y,j} = \frac{3\eta_{0,j}\zeta_{0,j}}{\sqrt{2}\eta_{0,j} - \zeta_{0,j}} \left\{ \ln\left[\frac{2\sqrt{2}G_j^b a_{S,j} a_{T,j} \tau_{0,j}^*}{\zeta_{0,j}}\right] + \ln\left|\dot{\epsilon}_{11}\right| \right\} \tag{B.12}$$

For adjusting model to experimental data, it important to express the yield stress in terms of temperature, T, ideal gas constant, R and the shear and pressure activation volumes i.e. $V_{s,j}$ and $V_{p,j}$, respectively. Let us substitute expressions for $\zeta_{0,j}$ and $\eta_{0,j}$ from *Equation C.1* into *Equation B.12* to get:

$$\sigma_{y,j} = \frac{6RT}{\sqrt{2}V_{s,j} - 2V_{p,j}} \left\{ \ln\left|\dot{\epsilon}_{11}\right| + \ln\left[\frac{\sqrt{2}V_{s,j}G_j^b a_{S,j} a_{T,j} \tau_{0,j}^*}{RT}\right] \right\} \tag{B.13}$$

It is convenient to write a contracted form of *Equation B.13* by setting:

$$A_j = \frac{\sqrt{2}V_{s,j}G_j^b a_{S,j} a_{T,j} \tau_{0,j}^*}{RT} \quad \text{and} \quad \dot{\epsilon}_{11} = \frac{\dot{\lambda}}{\lambda} \tag{B.14}$$

where $\lambda =$ stretch in 1-test direction and $\dot{\lambda} =$ rate of change of stretch.

Although the expression of *Equation B.13* was derived based on a compression test, a similar relationship will apply for a tensile test, except that the denominator of the slope term becomes: $\sqrt{2}V_{s,j} + 2V_{p,j}$. The '+' sign comes from the mean stress for a tensile test, expressed as: $\sigma_{m,j} = +\frac{1}{3}\sigma_{y,j}$, in the vicinity of yield. Therefore, the general form of the yield stress, for a $j-$process in the high stress regime becomes:

$$\sigma_{y,j}\bigg|_{high-stress} = \frac{6RT}{\sqrt{2}V_{s,j} \pm 2V_{p,j}}\left[\ln\left|\frac{\dot{\lambda}}{\lambda}\right| + \ln A_j\right] \tag{B.15}$$

The above is the same as *Equation 30*. The resulting equation of yield stress in the high octahedral shear stress (ratio) regime has a linear dependence with strain rate. The straight line is defined by a slope, M_j and intercept, C_j, for each $j-$process, where:

$$M_j = \frac{6RT}{\sqrt{2}V_{s,j} \pm 2V_{p,j}} \quad \text{and} \quad C_j = \frac{6RT}{\sqrt{2}V_{s,j} \pm 2V_{p,j}}\ln A_j$$

• **Case B: Compression at yield for the low stress regime**: Similar to the approach used for the high stress regime, here, we start the derivation of the dependence of yield stress on strain rate using the constitutive formulation of *Equation B.9*. Hence:

$$\tfrac{2}{3}\sigma_j = 2G_j^b a_{S,j} a_{T,j} a_{\sigma,j} \tau_{0,j}^*\left|\dot{\epsilon}_{11}\right| \tag{B.16}$$

40

Now we substitute the stress-shift factor equation for the low $\tau_{oct,j}^b/\zeta_{0,j}$ ratio (i.e. *Equation C.8*), into *Equation B.17* such that we obtain:

$$\frac{2}{3}\sigma_j \;=\; 2\left[\frac{2\dfrac{\tau_{oct,j}^b}{\zeta_{0,j}}}{\exp\left\{\dfrac{\tau_{oct,j}^b}{\zeta_{0,j}}\right\} - \exp\left\{-\dfrac{\tau_{oct,j}^b}{\zeta_{0,j}}\right\}}\right] G_j^b a_{S,j} a_{T,j}\tau_{0,j}^*\left|\dot{\epsilon}_{11}\right| \qquad \text{(B.17)}$$

We will now substitute *Equation B.11* into *Equation B.17* and cancel out common terms in both sides of the equation.

$$\frac{\cancel{2}}{\cancel{3}}\cancel{\sigma_j} \;=\; 2\left[\frac{\dfrac{\cancel{2}}{\cancel{3}}\sqrt{2}\dfrac{\cancel{\sigma_j}}{\zeta_{0,j}}}{\exp\left\{\dfrac{\sqrt{2}}{3}\dfrac{\sigma_j}{\zeta_{0,j}}\right\} - \exp\left\{-\dfrac{\sqrt{2}}{3}\dfrac{\sigma_j}{\zeta_{0,j}}\right\}}\right] G_j^b a_{S,j} a_{T,j}\tau_{0,j}^*\left|\dot{\epsilon}_{11}\right|$$

The resulting expression becomes:

$$1 \;=\; \frac{2\sqrt{2}G_j^b a_{S,j} a_{T,j}\tau_{0,j}^*\zeta_{0,j}^{-1}}{\exp\left\{\dfrac{\sqrt{2}}{3}\dfrac{\sigma_j}{\zeta_{0,j}}\right\} - \exp\left\{-\dfrac{\sqrt{2}}{3}\dfrac{\sigma_j}{\zeta_{0,j}}\right\}}\left|\dot{\epsilon}_{11}\right|$$

Taking the natural logarithm of both sides results, and re-arranging the equation results in:

$$\ln\left[\exp\left\{\frac{\sqrt{2}}{3}\frac{\sigma_j}{\zeta_{0,j}}\right\} - \exp\left\{-\frac{\sqrt{2}}{3}\frac{\sigma_j}{\zeta_{0,j}}\right\}\right] \;=\; \ln\left[\frac{2\sqrt{2}G_j^b a_{S,j} a_{T,j}\tau_{0,j}^*}{\zeta_{0,j}}\right] + \ln\left|\dot{\epsilon}_{11}\right|$$

Assume $W_j = \frac{\sqrt{2}}{3}\frac{\sigma_j}{\zeta_{0,j}}$ and A_j is same given in *Equation B.14*. Applying these to above equation gives:

$$\begin{aligned}
\ln\left(\exp(W_j) - \exp(-W_j)\right) &= \ln A_j + \ln\left|\dot{\epsilon}_{11}\right| \\
\ln\left(e^{W_j} - e^{-W_j}\right) &= \ln\left|A_j\dot{\epsilon}_{11}\right| \\
e^{W_j} - e^{-W_j} &= A_j\dot{\epsilon}_{11} \\
e^{2W_j} - A_j\dot{\epsilon}_{11}e^{W_j} - 1 &= 0
\end{aligned}$$

The above is a quadratic equation in terms of e^{W_j}. We obtain the roots of the quadratic equation thus:

41

$$e^{W_j} \quad = \quad \frac{A_j \dot{\epsilon}_{11}}{2} \pm \sqrt{\left(\frac{A_j \dot{\epsilon}_{11}}{2}\right)^2 + 1} \tag{B.18}$$

Taking the natural logarithm of both parts of *Equation B.18* results in:

$$W_j \quad = \quad \ln\left[\frac{A_j \dot{\epsilon}_{11}}{2} \pm \sqrt{\left(\frac{A_j \dot{\epsilon}_{11}}{2}\right)^2 + 1}\right] \quad \equiv \quad \frac{\sqrt{2}}{3}\frac{\sigma_j}{\zeta_{0,j}} \tag{B.19}$$

Finally, in the region around yield, $\sigma_j \equiv \sigma_{y,j}$, therefore, *Equation B.19* can be re-written such that we can obtain below, the relationship between yield stress and strain rate in the low-stress regime:

$$\sigma_{y,j}\Big|_{low-stress} \quad = \quad \frac{3\zeta_{0,j}}{\sqrt{2}} \ln\left[\frac{A_j \dot{\epsilon}_{11}}{2} \pm \sqrt{\left(\frac{A_j \dot{\epsilon}_{11}}{2}\right)^2 + 1}\right] \tag{B.20}$$

Of the two roots of the quadratic equation in *Equation B.18*, the experimentally realistic root for the quadratic equation will be that with a '+' as increasing strain rate, according to Eyring rate kinetics, should lead to increasing yield stress rather than reduction. Also, we re-write the $\zeta_{0,j}$ in terms of R, T and $V_{s,j}$, as well as ϵ_{11} in terms of stretch, λ. The result becomes:

$$\sigma_{y,j}\Big|_{low-stress} \quad = \quad \frac{6RT}{\sqrt{2}V_{s,j}} \ln\left[\frac{A_j}{2}\frac{\dot{\lambda}}{\lambda} \pm \sqrt{\left(\frac{A_j}{2}\frac{\dot{\lambda}}{\lambda}\right)^2 + 1}\right] \tag{B.21}$$

1 **Appendix C. The evolution of stress shift factor with relaxation time**

2   In order to understand the evolution of the stress shift factor on the relaxation times,
3 let us define the following shear-activation, $\zeta_{0,j}$ and pressure-activation, $\eta_{0,j}$ terms:
4

$$\zeta_{0,j} = \frac{2RT}{V_{s,j}} \quad \text{and} \quad \eta_{0,j} = \frac{RT}{V_{p,j}} \quad \text{for } j \in \{\alpha, \beta\}. \tag{C.1}$$

5   Incorporating the terms of *Equation C.1* into *Equation 16* results in:

$$a_{\sigma,j} = \frac{\dfrac{\tau_{oct,j}^{b}}{\zeta_{0,j}}}{\exp\left\{\dfrac{\sigma_m}{\eta_{0,j}}\right\}\sinh\left\{\dfrac{\tau_{oct,j}^{b}}{\zeta_{0,j}}\right\}}, \qquad \text{for} \quad j \in \{\alpha, \beta\} \tag{C.2}$$

6

7

8   *Equation C.2* is a nonlinear function of the bond-stretching octahedral shear stress ratio,
9 τ_{oct}^{b}/ζ_0 and the mean stress ratio, σ_m/η_0. Based on this nonlinear profile of the stress shift
10 factor (see *Equation C.2*), we can isolate two asymptotes to the stress shift profile, and these
11 correspond to high and low stress (bond-stretching octahedral shear stress ratio) asymptotes
12 which hereafter are referred to as the *high stress* and *low stress regimes* respectively. The
13 regimes are demarcated by the upper and lower bounds of the bond-stretching octahedral
14 shear stress ratio. We will explore these regimes in more detail such that we can deduce
15 simplified expressions of *Equation C.2* that are applicable at these extreme stress regimes.
16
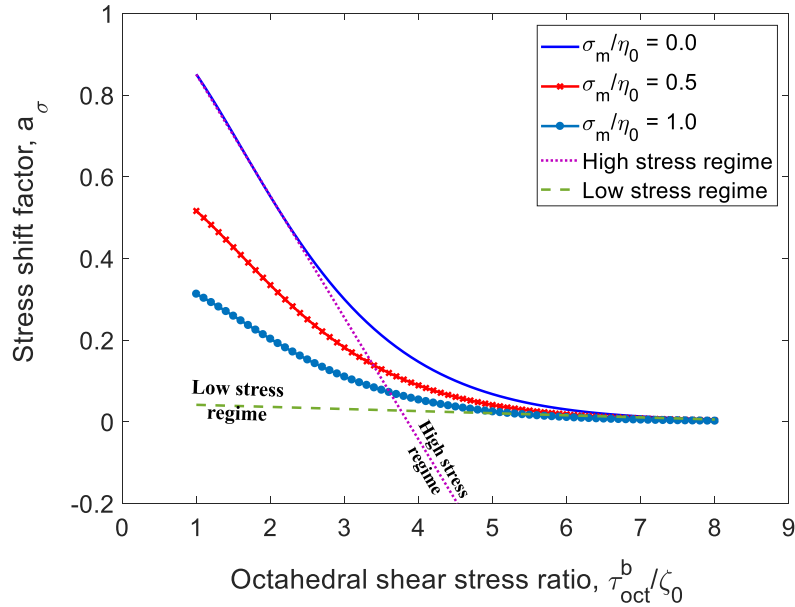
Figure C.12: The evolution of the stress shift factor, a_σ, with octahedral shear stress ratio, τ_{oct}^{b}/ζ_0 and mean stress ratio, σ_m/η_0. Notice the two asymptotes that correspond to high and low stress regimes.

High stress regime: In the high octahedral shear stress, $\tau^b_{\mathrm{oct},j}$, regime, the following inequality is true:

$$\frac{\tau^b_{\mathrm{oct},j}}{\zeta_{0,j}} \gg 1 \quad \text{for } j \in \{\alpha, \beta\}. \tag{C.3}$$

The expression of the hyperbolic sine function, in terms of exponentials for a variable, x is: $\sinh x = \frac{1}{2}(e^x - e^x)$. Using this expression with *Equation C.2* results in:

$$a_{\sigma,j}\Big|_{\text{high-stress}} = 2\frac{\tau^b_{\mathrm{oct},j}}{\zeta_{0,j}} \frac{\exp\left\{-\dfrac{\sigma_m}{\eta_{0,j}}\right\}}{\exp\left\{\dfrac{\tau_{\mathrm{oct},j}}{\zeta_{0,j}}\right\} - \exp\left\{-\dfrac{\tau_{\mathrm{oct},j}}{\zeta_{0,j}}\right\}} \tag{C.4}$$

Note that if $\dfrac{\tau^b_{\mathrm{oct},j}}{\zeta_{0,j}} \gg 1$, then $\exp\left\{-\dfrac{\tau_{\mathrm{oct},j}}{\zeta_{0,j}}\right\} \to 0$. Therefore, the stress shift factor (for the high stress regime) becomes:

$$a_{\sigma,j}\Big|_{\text{high-stress}} = 2\frac{\tau^b_{\mathrm{oct},j}}{\zeta_{0,j}} \exp\left[-\frac{\sigma_m}{\eta_{0,j}} - \frac{\tau^b_{\mathrm{oct},j}}{\zeta_{0,j}}\right] \tag{C.5}$$

Low stress regime: In the low octahedral shear stress, $\tau^b_{\mathrm{oct},j}$, regime, the following inequality is true:

$$\frac{\tau^b_{\mathrm{oct},j}}{\zeta_{0,j}} \ll 1 \quad \text{for } j \in \{\alpha, \beta\}. \tag{C.6}$$

Using similar exponential representation of the hyperbolic sine, and:

$$\text{for} \quad V_{p,j} \ll V_{s,j}, \quad \text{then} \quad \exp\left\{-\frac{\sigma_m}{\eta_{0,j}}\right\} \to 1, \tag{C.7}$$

the resulting expression for the low-stress regime stress shift factor becomes:

$$a_{\sigma,j}\Big|_{\text{low-stress}} = 2\frac{\tau^b_{\mathrm{oct},j}}{\zeta_{0,j}} \left[\exp\left\{\frac{\tau^b_{\mathrm{oct},j}}{\zeta_{0,j}}\right\} - \exp\left\{-\frac{\tau^b_{\mathrm{oct},j}}{\zeta_{0,j}}\right\}\right]^{-1} \tag{C.8}$$

These asymptotic representations of the effect of the stress shift factor on relaxation times has been used to derive the Ree-Eyring yield function formulation (for the proposed constitutive model). The details of this derivation are given in *Appendix B*.

Also, note that the *high stress regime* stress shift factor expression tends to describe the low strain rate or high temperature viscoelastic relaxation of the polymer while the *low stress regime* stress shift factor formulation defines the viscoelastic relaxation of the high strain rates or low temperature mechanical behaviour of the test polymer.
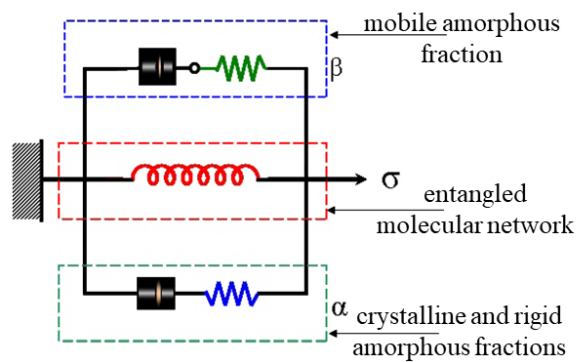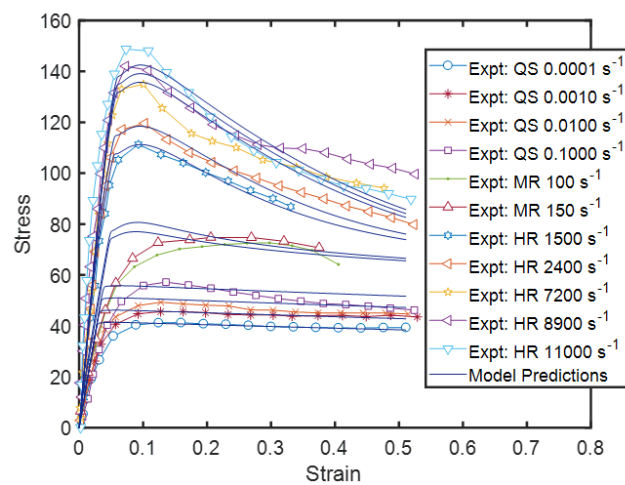
Manuscript number: Polymer-19-1360

Highlights

- 3D physically-based constitutive model for semicrystalline polymers
- The model is particularly suitable to melt-crystallized semicrystalline polymers
- The model is based on two-process viscoelastic relaxations of polymer's phases
- The model captures rate effects, adiabatic heating, structural rejuvenation
- The model is applicable for impact dynamics investigations